Chem Soc Rev

Check for updates

Anion···anion self-assembly under the control of σ- and π-hole bonds

Andrea Pizzi, [ID] Arun Dhaka, [ID] Roberta Beccaria [ID] and Giuseppe Resnati [ID]*

The electrostatic attraction between charges of opposite signs and the repulsion between charges of the same sign are ubiquitous and influential phenomena in recognition and self-assembly processes. However, it has been recently revealed that specific attractive forces between ions with the same sign are relatively common. These forces can be strong enough to overcome the Coulomb repulsion between ions with the same sign, leading to the formation of stable anion···anion and cation···cation adducts. Hydroden bonds (HBs) are probably the best-known interaction that can effectively direct these counterintuitive assembly processes. In this review we discuss how σ-hole and π-hole bonds can break the paradigm of electrostatic repulsion between like-charges and effectively drive the self-assembly of anions into discrete as well as one-, two-, or three-dimensional adducts. σ-Hole and π-hole bonds are the attractive forces between regions of excess electron density in molecular entities (*e.g.*, lone pairs or π bond orbitals) and regions of depleted electron density that are localized at the outer surface of bonded atoms opposite to the σ covalent bonds formed by atoms (σ-holes) and above and below the planar portions of molecular entities (π-holes). σ- and π-holes can be present on many different elements of the p and d block of the periodic table and the self-assembly processes driven by their presence can thus involve a wide diversity of mono- and di-anions. The formed homomeric and heteromeric adducts are typically stable in the solid phase and in polar solvents but metastable or unstable in the gas phase. The pivotal role of σ- and π-hole bonds in controlling anion···anion self-assembly is described in key biopharmacological systems and in molecular materials endowed with useful functional properties.

Key learning points

1. The distribution of electron density at the surface of bonded atoms is anisotropic.
2. In many polyatomic anions (*e.g.*, IO_4^-, NO_3^-, $PdCl_4^{2-}$, and $AuCl_4^-$), atoms having regions with depleted electron density (electrophilic sites) and excess electron density (nucleophilic sites) may both be present.
3. Attractive interactions between these electrophilic and nucleophilic sites can drive the formation of anion···anion adducts.
4. These adducts can exist as stable species in the solid form or in solution and occasionally also in the gas phase.
5. Such anion···anion interactions have significant impacts on compounds as relevant as ATP and nonlinear optical materials.

1. Introduction

Molecular recognition and self-assembly are the holistic result of the balanced combination of a multitude of electronic and geometric features of interacting units. The electrostatic attraction between charges of opposite sign is one of the most common and influential effects which can bring molecular entities close together and drive their assembly into

NFMLab, Department of Chemistry, Materials, Chemical Engineering "Giulio Natta", Politecnico di Milano, via Mancinelli 7, I-20131 Milano, Italy. E-mail: giuseppe.resnati@polimi.it

well-organized adducts.[1] The repulsion between charges of the same sign (like-charges) is equally important and tends to separate anions from each other. The self-assembly of anions into discrete or infinite adducts can occur only if specific attractive forces are present and can successfully overcome the Coulombic anion···anion repulsion.[2,3] It might thus be expected that these phenomena are exceptional, but it has been reported that a variety of natural anions, *e.g.*, malonate,[4] citrate,[5] and carboxylate forms of amino acids,[6] can aggregate and give rise to short anion···anion contacts.[7] Indeed, in biological systems, the presence of anion···anion interactions is fairly common. Also, synthetic anions (*e.g.*, hexacyanoferrate[3,8] and nitroprusside anions[9]) self-assemble

under different conditions.[10] In this review, we will describe how σ-[11,12] and π-hole[13,14] interactions can effectively counteract the electrostatic repulsion between like charges; specifically, we will describe how they enable the self-assembly of anions into discrete adducts or 1D, 2D, and 3D supramolecular architectures.[15]

The ability of the hydrogen bond (HB) to overcome the Coulombic repulsion between protic hydroxyanions and to drive their self-assembly into stable anion···anion adducts has been recognized since long ago. Anion···anion adducts formed by $H_2PO_4^-$ are of paramount importance. The dimerization of this anion in water solution and the value of the association constant were reported as early as 1969.[16] The selectivity of phosphate binding proteins for phosphate over sulphate is ensured by the ability of hydroxy group(s) of phosphate anion to bind a carboxylate residue present, at physiological pH, in the protein active site.[17] ADP and ATP synthesis and hydrolysis are ubiquitous processes and of

immense relevance in living organisms; the involvement of their phosphoric residues in the formation of anion···anion short contacts under the control of HB plays a key role in these processes.[18–20] The HB driven self-assembly of monoanions of di- and poly-carboxylic acids of biopharmacological relevance is a widespread phenomenon.[4,5] The versatility and effectiveness of the HB in enabling anion···anion adducts formation is confirmed by the formation of not only homomeric adducts (*e.g.*, starting from HCO_3^-, $H_2PO_4^-$, $H_2AsO_4^-$, HSO_4^-),[21,22] but also heteromeric trimers (HSO_4^-···$H_2PO_4^-$···HSO_4^-)[23] and dianions dimers (HPO_4^{2-}···HPO_4^{2-} and $HAsO_4^{2-}$···$HAsO_4^{2-}$).[22]

σ- and π-hole interactions complement the potential of HB in directing anion···anion self-assembly by extending this process to anions wherein no hydroxy group is present. The versatility and effectiveness of σ/π-hole interactions in forming anion···anion adducts are probably as impactful as those of HBs. For instance, discrete adducts or infinite supramolecular

Dr Andrea Pizzi is an Assistant Professor at Politecnico di Milano, in the Laboratory of Nanostructured Fluorinated Materials (NFMLab). His PhD thesis, under the supervision of Prof. Pierangelo Metrangolo, was focused on halogen bonding in peptides and proteins. His research interest is in the field of supramolecular chemistry based on σ-hole interactions, aimed at investigating the functioning of catalysts and

Andrea Pizzi

obtaining new biomimetic materials. He is currently investigating the role of anion···anion interactions in proteins and small molecules in the solid state.

Dr Arun Dhaka is a MSCA post-doctoral researcher at Politecnico di Milano, in the Laboratory of Nanostructured Fluorinated Materials (NFMLab). His Phd work on condensed matter was carried out under the supervision of Dr Marc Fourmiguè at Universitè de Rennes, France. His research interests broadly encompass the field of crystal engineering and molecular materials, with a focus on self-assembly processes

Arun Dhaka

driven under the control of σ-hole interactions, creating novel crystalline solids. He is currently investigating anion···anion interactions in molecular solids.

Roberta Beccaria is a PhD candidate in the Laboratory of Nanostructured Fluorinated Materials (NFMLab) at Politecnico di Milano. She obtained her Master's degree in Chemistry at the Università degli Studi di Torino in 2022 with a thesis on pharmaceutical cocrystals. Her areas of interest in research concern supramolecular chemistry and crystal engineering, with a particular focus on analytical techniques for assessing the

Roberta Beccaria

formation of self-assembled systems mainly in the solid (X-ray analyses) but also in solution (NMR).

Giuseppe Resnati is Professor of general chemistry for materials and nanotechnologies at the Politecnico di Milano. His interest in fluoroorganic chemistry prompted him to start the Laboratory of Nanostructured Fluorinated Materials (NFMLab) to investigate the asymmetric synthesis of fluorinated compounds and the chemistry of fluorous oxydizing agents. In the last decades, he focused on recognition and self-assembly processes driven by

Giuseppe Resnati

halogen, chalcogen, and pnictogen bonds as well as by analogous interactions involving a d block element as the electrophile. Anion···anion interactions are included in this latter area of interest.

This journal is © The Royal Society of Chemistry 2024

Chem. Soc. Rev., 2024, **53**, 6654–6674 | **6655**

architectures have been obtained through the self-assembly of mono- and dianions as different as IO_3^-,[24] MnO_4^-,[25] $AuCl_4^-$,[26] $XeCl_5^-$,[27] $PdCl_4^{2-}$,[28] and $Se_2O_5^{2-}$.[29]

The halogen bond (HaB), an attractive and directional bonding where group 17 elements behave as electrophiles,[30] is the first identified and best studied σ-hole interaction. The history of HaB dates back two hundred years[31] and its present understanding is the result of many studies wherein different rationalization models were proposed.[32] The struggle to understand the phenomenon is emblematically declared by the twenty descriptive phrases listed in 1968 by H. A. Bent[33] to indicate what is now named HaB.[34–40] The wording "bumps-in-hollows" and "pair-pocket" are two of the descriptors mentioned by Bent, which closely resemble the hole model adopted here. Importantly, in their seminal paper published on the HaB in 1996, F. H. Allen *et al.* stated that "The attractive nature of the interaction is mainly due to electrostatic effects, but polarization, charge-transfer, and dispersion contributions all play an important role in causing interpenetration of van der Waals volumes".[41]

The chalcogen bond (ChB), a bonding interaction wherein the electrophile is a group 16 element,[42] is the second most impacting σ/π-hole interaction.[43,44] Similar to the HaB, the present understanding of this interaction has developed through a rather patchy course. The contributions focussing on the charge-transfer[33,35,36] and geometric[37,45] viewpoints were important in constructing the present-day ChB concept, but the topic boomed and was clearly defined[42] only after modelling based on the electrostatic standpoint was proposed.[46] It is commonly accepted that Allen's generalization on the HaB equally holds for the ChB and other σ/π-hole interaction.[47–49]

In order to further present the basics of σ/π-hole interactions with a focus on those affording anion···anion adducts, we will not delve into the details of all theoretical models that have been proposed to rationalize these interactions and which contemplates the presence of covalent[50] and dative[51] components. Different computational methods give different relative weights to the different components of σ/π-hole interactions and providing a critical assessment of related problems is out of the scope of this review.[52] We will concentrate only on the electrostatic and the charge-transfer models as experimental evidence supports their relevance in all σ/π-hole bonds. Emphasis will be given to the electrostatic viewpoint[53] as it is the most frequently employed one and the pictures representing the molecular electrostatic potential (MEP) are very intuitive and have a strong communicative effectiveness.

The basis of the electrostatic model of σ/π-hole interactions is the anisotropic distribution of the electron density in bonded atoms. This anisotropy determines the presence of regions of depleted electron density that are localized along the elongation of the σ covalent bonds formed by atoms (σ-holes) or above and below a planar region of a molecular entity (π-holes). According to this perspective, the σ-[11,12] and π-hole bonds[13,14] are the short and attractive contacts between these regions, acting as electrophilic sites (Lewis acidic sites), and regions of excess electron density (*e.g.*, lone pair orbitals or π covalent bonds), acting as nucleophilic sites (Lewis basic sites). The
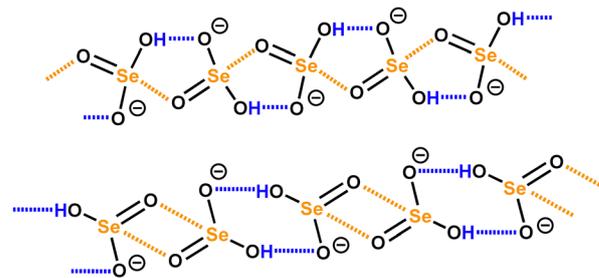
Scheme 1 Infinite chains formed by $HSeO_3^-$ anions under synergistic action of ChBs and HBs.[29]

linear and orthogonal geometries of σ- and π-hole bonds are a consequence of the location of σ- and π-holes in the outer regions of atoms and molecules.

When a σ covalent bond is formed, the accumulation of the electron density in the bond region occurs at the cost of a depletion outside the bond, this depletion aligns collinearly with the bond and generates the σ-hole (electrostatic viewpoint). But upon the formation of a σ covalent bond, an antibonding (higher energy) and non-occupied orbital (σ*) is also formed. An attractive interaction occurs when this empty orbital (electrophilic site) overlaps with a lone-pair or a π-bond orbital (nucleophilic sites) and a transfer of electron density ensues (n/π → σ* charge-transfer interaction).

Similarly, an attractive interaction results from the overlap and transfer of electron density between a lone-pair or a π-bond orbital and an empty π* orbital. Understanding the distribution of electron density in molecules similar to the approach used by electronic engineers when talking about electron holes, the empty σ*/π*orbitals that can accept electron density from an occupied orbital (and indeed do so) can be considered σ/π-holes and the resulting interactions can be named σ/π-hole bonds. According to the charge-transfer rationalization, the linear and perpendicular geometries of σ- and π-hole bonds are a consequence of the localization and orientation of the antibonding orbitals accepting electron density from the nucleophile.

Finally, it may be useful to observe that the anion···anion self-assembly driven by HBs and σ/π-hole bonds are not mutually exclusive processes but can occur concomitantly and cooperate in constructing anionic supramolecular architectures. This is the case, for instance, with hydroselenite anions $(HSeO_3^-)$[29] in hybrid organic–inorganic salts which form structurally different infinite chains where anions are doubly pinned to each other by a synthon composed of one HB and one ChB (Scheme 1, top) or where dimers bonded *via* two H···O HBs are connected *via* two Se···O ChBs (Scheme 1, bottom).

2. Generalities on anion···anion adducts in the solid, liquid, and gas phases

In isolated anions, σ- and π-holes are found at the expected positions and the MEP value is also negative in these regions,

6656 | *Chem. Soc. Rev.*, 2024, **53**, 6654–6674

This journal is © The Royal Society of Chemistry 2024

while less negative than elsewhere. This may lead to the expectation that the approach of an anion to these holes is electrostatically disfavoured, but, as exemplified onwards, this may not always be the case. In general, attractive interactions between like-charges[54] can be treated as Coulombic if electrostatics and polarization are both considered.[55] In this analysis, dispersion is included as part of polarization.[56] The electrostatic potential of any region in a molecular entity creates an electric field which affects the charge distribution in any other region of the same and nearby molecular entities (polarization). The electrostatic potential of two, or more, units in an adduct is thus different from that of the same units when isolated and in their ground state. If the ground state potentials of two isolated units have the same sign and one of them is weak, this polarizing force is enough to overcome the ground state electrostatic repulsion of the isolated units and to enable attractive interactions. In anion···anion adducts, the interacting region with the locally more negatively charged potential functions as the donor of electron density (nucleophile) while the interacting region with the locally less negatively charged potential is still capable of functioning as the acceptor of electron density (nucleophile).[57]

In the solid state and in solution, anions are not present as isolated species as they are in close proximity to surrounding cations and solvent molecules. The MEP of anion–cation pairs (computed either in the crystallographic or optimized geometry) show the presence of σ/π-holes on the anionic units where the electrostatic potential is less negative than in isolated anions or it is even positive, making them suitable to interact attractively with atoms having a negative potential (Fig. 1 and 2).[25,26]

It is also important to note that, following Bader's recommendation[58] MEPs are routinely calculated using the 0.001 a.u. isovalue as it embraces ca. 99% of the electron density and provides a quite good estimate of the van der Waals surface. But the anion···anion interactions considered in this review occur at distances shorter than the van der Waals radii and the electrostatic component of their nature may be better estimated by using surfaces smaller than the van der Waals one, i.e., by considering isovalues greater than 0.001 a.u. The MEP values at σ- and π-hole sites progressively increase with the isovalue,[26] particularly when they approach the nuclei of atoms. Indeed, at distances comparable to those of the observed anion···anion interactions they may become positive when they are negative if considered on the 0.001 a.u. isovalue surface (Fig. 1).

According to the charge-transfer viewpoint, in anion···anion adducts, the superposition between an occupied orbital of the anion acting as the donor of electron density and an empty antibonding orbital in the hole region of the other anion results in a charge-transfer stabilization which, depending on the adduct and the adopted modelling tool, can be a major attractive component in the interactions.[50,59] Importantly, this stabilizing force acts independent of the like-charge of the two anions and of the electrostatic potential in the regions involved in the interaction.
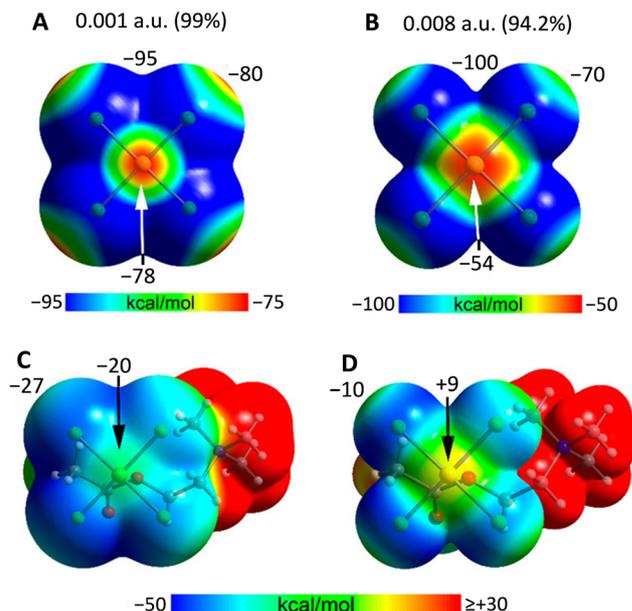

Fig. 1 MEP surfaces of the isolated $AuCl_4^-$ anion and its acetylcholine ion pair[26] using 0.001 a.u. (A) and (C) and 0.008 a.u. (B) and (D) isovalues at the PBE0-D3/def2-TZVP level of theory. Some values of the surface electrostatic potential are given in kcal mol^{-1} at the given points.

The ability of anions to form anion···anion adducts in the condensed phases is also affected by the overall interactional landscape in which they are involved. Specifically, interactions formed by anions with electrophiles (e.g., the HBs or HaBs formed by oxygen atoms of oxoacid anions with positively charged hydrogen atoms of cationic units or with electrophilic halogen atoms) dissipate the net negative charge of the anions; this increases their surface electrostatic potential and helps in the possible formation of close and attractive contacts with other anions.[60,61] The stronger and more numerous these anion–electrophile interactions are, the more extended and less negative, or more positive, the anion σ/π-hole(s) are, and the more favoured the formation of stable anion···anion adducts is.

σ/π-Hole interactions frequently allow anion···anion adducts to be metastable species in the gas phase, namely, the diagram of the binding energies of the two anions vs. the anions separation show a local minimum which is positive. Calculations on the 32 dimers formed by the four halide anions with the eight anionic HaB donors depicted in Table 1 reveal that in the gas phase 18 of them are thermodynamically unstable but kinetically stable with respect to the isolated species and the others dissociate spontaneously (Table 1 and Fig. 3).[62] The relatively large set of data allow making some general observations. The local minimum of the dimer binding energy can be fairly deep. The largest dissociation barriers are found for the most stable minima, while the smallest ones are obtained for the least stable minima. Iodocarbons form more stable dimers than structurally analogous bromocarbons and as far as the donor of electron density is concerned the binding energies follow the following order: $F^- < Cl^- < Br^- < I^-$.[63]
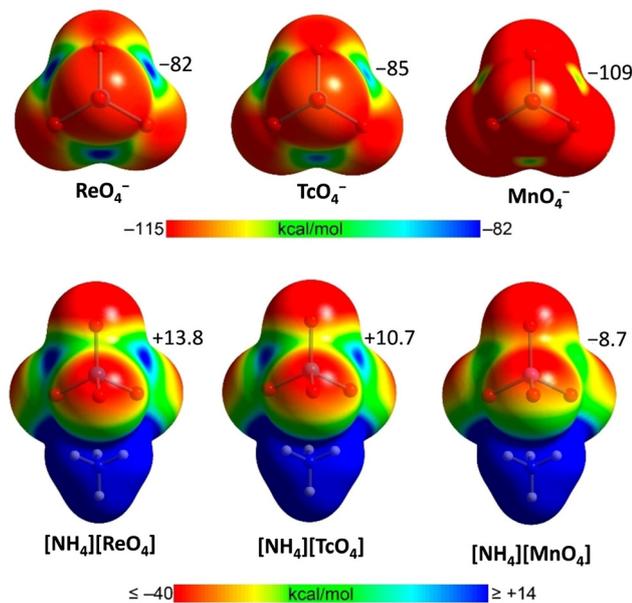
This journal is © The Royal Society of Chemistry 2024

Chem. Soc. Rev., 2024, 53, 6654–6674 | 6657

Fig. 2 MEP surfaces of MaO_4^- (Ma = Mn, Tc and Re) anions and their ammonium salts[25] at the PBE0-D3/def2-TZVP level of theory. The values at σ-holes are given in kcal mol^{-1}.

Fig. 3 Binding energy (E_b, kJ mol^{-1}) vs. Br/I···halide anion distance of 4-bromo- and 4-iodo-benzoate complexes in the gas phase.[62]

In solution, the dielectric environment of polar solvents effectively lowers the electrostatic repulsion between like-charges, stabilizing the anion···anion adducts, and the local minimum in the diagram of the binding energies of the two anions vs. their distance decreases in all cases and frequently becomes negative (Table 1), indicating that the interactions become thermodynamically stable. Computational analyses[24,25,64–66] and experimental results[67] on various systems consistently show that the stabilizing effect increases with the dielectric constant of the solvent. UV-vis analyses of solutions containing an anionic and iodinated cyclopropenylium-based donor of HaB and chloride, bromide, or iodide anions gave experimental proof of the presence of complexes between the organic anion and all three inorganic anions. Stabilities of
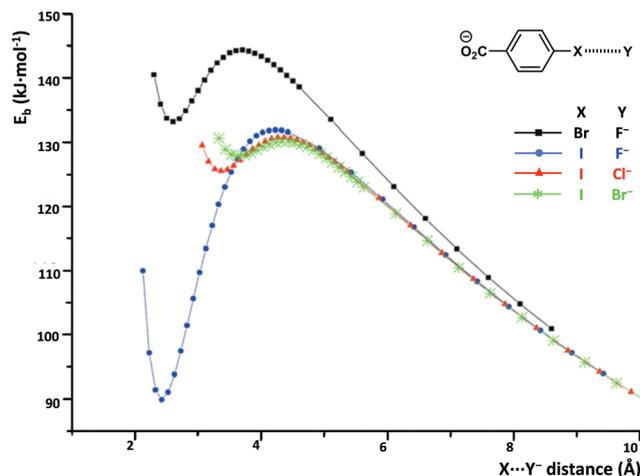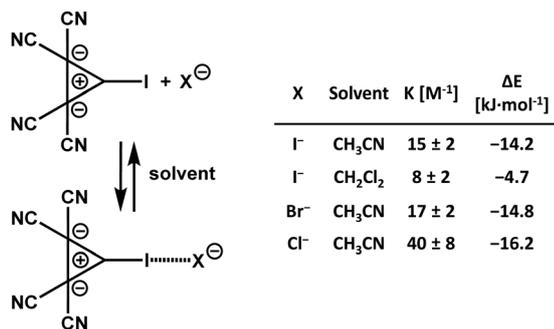
these adducts are comparable to those formed when the same halides bind to common neutral HaB donors, e.g., bromo- and iodo-alkanes and -arenes (Scheme 2).[67] These findings confirm that the HaBs between anionic HaB donors and halide anions are strong enough to overcome the Coulombic repulsion between like-charges, even in solution.[68] Moreover, they experimentally support the numerous computational studies which suggest that a weak covalent component contributes to the formation of halogen bonded complexes between two anions.

The dielectric constant of any crystalline solid is unknown, but it can be expected that the ionic environment in a crystalline salt is even more effective than a polar solvent in lowering the Coulombic repulsion between anions and in stabilizing anion···anion adducts. This may explain why numerous structures in the Cambridge structural database (CSD)[69] show numerous short anion···anion contacts which can be rationalized as σ/π-hole attractive interactions. It also supports the general ability of σ/π-hole interactions between anions to function as reliable tools in crystal engineering.

Table 1 Binding energy (E_b, kJ mol^{-1}) and interaction separation (in parenthesis, pm; characters in italic are for water solution) for the halogen bonded anion···anion adducts ^-O_2C−spacer−X···halide anion[62]

Halide anion	X = Br	I	Br	I	Br	I	Br	I
Gas phase								
F$^-$	133.2 (259.7)	89.8 (241.9)	147.4 (268.2)	109.9 (247.9)	155.9 (272.3)	118.2 (248.9)	115.9 (233.3)	58.5 (227.8)
Cl$^-$	—	125.6 (335.9)	—	137.8 (349.9)	—	143.3 (356.9)	140.0 (328.5)	111.9 (310.8)
Br$^-$	—	127.9 (362.6)	—	138.6 (385.4)	—	—	140.4 (366.9)	116.8 (335.6)
I$^-$	—	—	—	—	—	—	—	120.2 (366.2)
Water solution								
F$^-$	−2.5 (286.5)	−16.28 (262.6)	2.0 (309.9)	−5.8 (279.2)	0.9 (413.7)	−2.4 (288.1)	−10.0 (263.9)	−34.0 (241.4)
Cl$^-$	—	−7.9 (342.5)	—	−3.3 (357.6)	—	−2.2 (366.7)	−6.5 (330.5)	16.2 (321.1)
Br$^-$	—	−8.1 (358.0)	—	−3.3 (372.2)	—	—	−7.2 (345.5)	−15.9 (339.2)
I$^-$	—	—	—	—	—	—	—	−15.4 (361.7)

6658 | Chem. Soc. Rev., 2024, 53, 6654–6674

This journal is © The Royal Society of Chemistry 2024

Scheme 2 Formation of halogen bonded adducts between an anionic and iodinated bis(dicyanomethylene)cyclopropanide derivative and halide anions.[67]

Finally, in order to evince how the overall molecular structure of a polyatomic anion affects its ability to function as the donor of σ-hole interactions and determines the stability of the adducts formed with other anions, a computational study was performed on anion···anion dimers formed by ω-iodocarboxylates wherein the iodine atom and the carboxylate group are separated by polyyne, polyene, or polymethylene chains of different lengths. As the distance between the iodine (the HaB donor atom, $i.e.$, the electrophilic site) and the carboxylate group (the HaB acceptor site, $i.e.$, the nucleophilic site) increases, the energy of the dimer tends to decrease with respect to the two separated anions as reported in Scheme 3 for dimers between iodocarbon anions and a chloride anion.[70] While shorter spacing chains produce anion···anion dimers which are metastable in the gas phase (positive binding energies), the longer ones can yield stable dimers (negative binding energies). Polymethylene chains are more effective in stabilizing the anion dimers than polyene chains with the same number of carbon atoms.

3. Adducts assembled by σ−hole interactions

Donors of electron density can engage in attractive interactions when they approach σ/πholes centred on a wide diversity of elements. This also applies to the subset of interactions wherein the donor and the acceptor of the electron density are both anions. This section and the following one record the
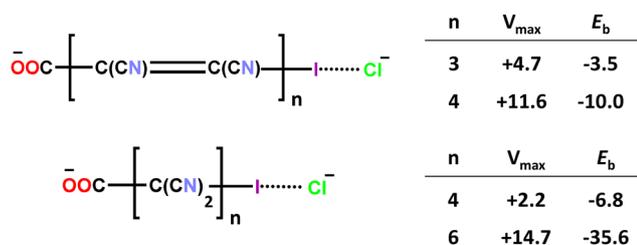
Scheme 3 Electrostatic potential at the σ-hole of iodine (V_{max}) in some ω-iodocarboxylates and binding energy (E_b) of these anions with chloride anions; both values are in kcal mol^{-1}.[70]

anion···anion adducts formed under the influence of σ- and π-hole interactions by dividing them in subsections devoted to systems wherein the element hosting the hole belongs to the p or d blocks of the periodic table.

3.1. σ-Hole interactions at p block elements

Boron, aluminium, gallium, indium, and thallium, the five common elements of group 13, are collectively named triels (Trs) and the σ/π-hole interactions involving them as electrophilic atoms are usually designated as triel bonds (TrBs).[71] In the solid state, their tetrahalide anions (TrX$_4^-$) adopt a tetrahedral geometry and structures are present in the CSD wherein these anions are assembled into X$_4$Tr$^-$···TrX$_4^-$ adducts (Tr = B,[72–75] Al,[76] In,[77,78] and Tl;[79] X = F,[72–75] Cl,[76,77,79] and Br[78]) via one or more Tr···X short contacts between different anions. A systematic study of several triel tetrahalides confirmed computationally the attractive nature of these TrBs.[80] This study showed that the Coulomb repulsion is counteracted by large polarization energies and the formed dimers are typically metastable in the gas phase and stable in solution. Bond paths and bond critical points (CPs) were frequently observed for the Tr···X TrBs. Similar to the σ/π-hole interactions involving neutral units, the strength of inter-anion TrBs increases with the atomic weight of the Tr atom.

Computational analyses at different levels indicate that heteromeric anion adducts can be formed on interaction with CN$^-$ anions. Specifically, for the tetrachlorides of the four heaviest triels (Al, Ga, In, and Tl), the more stable adducts are two structurally different Cl$_4$Tr$^-$···CN$^-$ complexes (encoded as E and A isomers, respectively, Table 2), both of which have carbon of the cyano group positioned close to the triel and both adopt a distorted trigonal bipyramidal geometry with the cyano group in the equatorial or axial position.[81] Two other complexes with the nitrogen of the cyano group close to the triel are less stable. When the Cl$_4$Tr$^-$ and CN$^-$ anions come close to each other, the tetrahedral geometry of the isolated TrCl$_4^-$ anion restructures and forms either the E or A isomers, locating the four chlorine atoms in a distorted see-saw geometry or in a pseudo trigonal pyramidal geometry. The energetic cost of

Table 2 Binding energy (E_b, kcal mol^{-1}) for Cl$_4$Tr$^-$···CN$^-$ complexes in gas and water phases.[65] One set of values for a complex with ammonia as a neutral TrB acceptor is reported for the sake of comparison

	$E_{b(gas\ phase)}$		$E_{b(water\ sol.)}$	
	MP2	CCSD(T)	MP2	CCSD(T)
E isomer				
Cl$_4$Al$^-$···CN$^-$	48.78	50.99	−9.11	−6.63
Cl$_4$Ga$^-$···CN$^-$	49.10	51.53	−8.54	−5.80
Cl$_4$In$^-$···CN$^-$	36.98	39.13	−17.06	−14.59
Cl$_4$Tl$^-$···CN$^-$	37.78	40.23	−15.61	−12.72
A isomer				
Cl$_4$Al$^-$···CN$^-$	48.85	50.98	−8.81	−6.47
Cl$_4$Ga$^-$···CN$^-$	50.59	52.89	−6.45	−3.92
Cl$_4$In$^-$···CN$^-$	37.28	39.31	−16.01	−13.64
Cl$_4$Tl$^-$···CN$^-$	38.13	40.44	−13.85	−11.22
Cl$_4$Tl$^-$···NH$_3$	−22.07	−19.95	−6.01	−4.43

these rearrangements, while smaller for the larger triels, is non-minor in all cases. These restructurings nevertheless occur as they help complex formation by inducing a much more positive, or less negative, electrostatic potential at the positions that are to be occupied by the cyano group in the complexes. The $Cl_4Tr^-\cdots CN^-$ dimers are formed as the resulting σ-hole TrBs between the $TrCl_4^-$ and CN^- anion are strong enough to overcome the long-range Coulombic repulsion between their like charges. In the gas phase, these complexes are characterized by positive binding energies, but they are metastable, namely, an energy barrier opposes their dissociation. In water solution they become stable and the binding energies are more negative than those of some complexes wherein anions interact with neutral donors of electron density (e.g., $Cl_4Tr^-\cdots NH_3$), consistent with the general tendency of anionic donors of electron density to form stronger σ-hole interactions than neutral donors.

A computational study rationalizes[82] the $Cl_4Pn^-\cdots CN^-$ complexes (Pn = P, As, and Sb) as systems formed under the control of the pnictogen bond (PnB), the σ/π-hole interaction wherein the electrophilic atom is the group 15 element.[83] On approach of the CN^- anion, $PnCl_4^-$ rearranges from its see-saw geometry, the preferred conformation in the solid and gas phases, to the square geometry and a minimum on the potential energy surface is found for complexes with the CN^- ion in apical position with the carbon atom pointing to the pnictogen atom. These complexes are metastable in the gas phase, meaning their dissociation requires the two monoanions to pass an energy barrier, but in water solution they are more stable than the isolated monoanions, as it happens in several other systems. These polyanion complexes can be rationalized not only as systems formed under the control of σ-hole PnBs involving the $PnCl_4^-$ anion in the see-saw conformation, as described above, but also as systems formed under the control of π-hole PnBs involving the $PnCl_4^-$ anion in the rearranged square conformation. An analysis of the CSD confirms the tendency of the pnictogen atom in PnX_4^- monoanions (Pn = As, Sb, Bi; X = F, Cl, and occasionally Br, I) and in related species (e.g. $Pn_2X_7^-$) to form short contacts with other anions (e.g., with X^- or with another PnX_4^-) and to form supramolecular anionic adducts having quite different structures and charges.[84–87]

Experimental and theoretical results show that the self-assembly of anion···anion adducts can be driven by σ-hole ChBs involving S, Se, and Te atoms of both organic and inorganic anions. Dithieno[3,2-b:2′,3′-d]thiophene and its analogues can bind anions via convergent bidentate ChBs.[88] The ChB driven binding of a chloride anion by some dithieno [3,2-b:2′,3′-d]pyrroles bearing a deprotonated dicyanomethylene pendant on the bridging nitrogen, and by the diselenopheno and ditelluropheno analogues, has been studied computationally.[89] The stabilizing charge-transfer, polarization, and dispersion components of the binding energy become monotonically more and more negative as the anions get together. As expected from classic electrostatics, the electrostatic component experiences a Coulombic repulsion that

increases with the shortening of the $Ch\cdots X^-$ distance. This happens before reaching a given threshold (the barrier separation), and after passing this threshold it decreases as the $Ch\cdots X^-$ distance shortens and at quite close separations it becomes even more favourable than some other energy components. As a result, characteristic energy minima are present in the diagrams of the binding energy vs. the $Ch\cdots X^-$ distance for all the examined systems. The local minimum of the dimer binding energy is positive in most dimers (kinetically stable adducts), it decreases when moving from S, to Se, to Te, and it is negative for some of the studied ditelluropheno dimers (thermodynamically stable adducts). An analogous dependence of the stability of anion···anion adducts assembled by σ/π–hole interactions on the polarizability and electronegativity of the atom hosting the hole has been described above for triel bonded systems and will be discussed further for systems involving elements of groups 7 and 17. Clearly, the general tendency of σ/π-hole interactions involving neutral units to become more stabilizing with the increase in the polarizability and the decrease in the electronegativity of the atom hosting the hole, is equally applicable in σ/π-hole interactions involving anionic units.

Approximately one fourth of the CSD structures that contain the $HSeO_3^-$ unit shows the presence of anion···anion adducts assembled via $Se\cdots O$ ChBs between two anions.[90–92] The effectiveness of this interaction and its reliability in crystal engineering has been proven by the design of chalcogen bonded anion···anion dimers and infinite chains (Scheme 1).[29] Interestingly, the same paper describes that selenium is a quite strong ChB donor also in the diselenite dianion ($Se_2O_5^{2-}$) as it forms two-dimensional (2D) anion···anion architectures via $Se\cdots O$ ChBs which can be 302.9 pm long, characterized by a normalized contact[93] as small as 0.88 (Fig. 4). A combined quantum theory of atoms-in-molecules (QTAIM) and noncovalent interaction plot (NCIPlot) analysis identifies a bond path and a bond CP for the short $Se\cdots O$ contacts observed in the crystals. A green and bluish reduced density gradient (RDG) isosurface characterizes these interactions so that their attractive nature is confirmed, in spite of the overall Coulombic repulsion between the two anions.

Structures in the CSD[94,95] and computational studies[96] indicate that the aryl-tetrahalotellurate anion and the alkyl-tetrahalo analogues as well as the corresponding selenium and sulfur species (aryl/alkyl-ChX_4^-, Ch = S, Se, and Te; X = Cl, Br, and I) form dimers through the antiparallel pairing of the Ch–X moiety of different anions. The main attractive components of these ChBs are polarization and charge-transfer (from the halogen lone pairs to the chalcogen), and the formed dimers are metastable in the gas phase and stable in water solution.

The casuistry of anion···anion adducts assembled via HaBs is wider and more diversified than that of adducts assembled via other σ-hole interactions,[15] consistent with HaBs being the most extensively studied σ-hole bond.

Polyiodides are well-known systems which have received great attention thanks to their useful applications and highly diversified structures. As stated by L. Kloo in his review

6660 | Chem. Soc. Rev., 2024, 53, 6654–6674

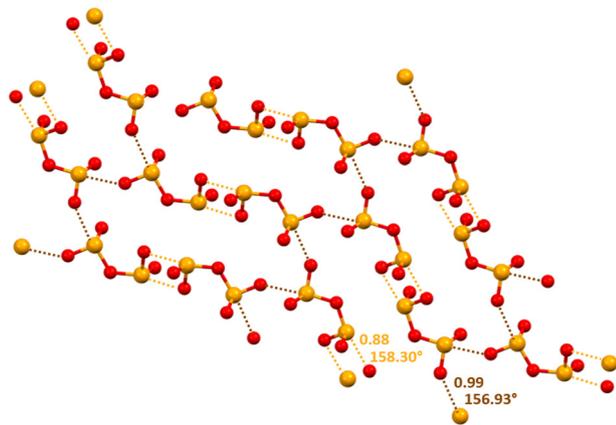This journal is © The Royal Society of Chemistry 2024

Fig. 4 Partial representation (ball and stick, Mercury 2022.1.0) of the 2D net assembled *via* ChBs in a salt between diprotonated diazabicyclooctane and diselenite dianion (Refcode BOGWEG).[29] Short and long ChBs are ocher and brown dotted lines; ChB angles and Nc values are reported close to the interactions. Colour code: red, oxygen and orange, selenium.

"Examples of everything from very simple discrete units to one-dimensional chains and complicated two and three-dimensional networks all occur."[97] To a lesser extent, this is also true for other homo- and heteromeric polyhalides.[98] Even the formation of as extreme systems as stable $Cl^-\cdots Cl^-$ dimers has been reported.[99] Some polyhalide anions result from the interaction of an halide anion with one or more dihalogen molecules; some others are formed *via* the interaction of two or more (poly)halides and here we will discuss these latter systems only. The bonding nature in polyiodides has been the subject of much theoretical speculation and traditionally their formation has been rationalized *via* the donor–acceptor and multicenter bonding modellings. Often their geometric features are consistent with those expected for σ-hole adducts and recent theoretical studies have confirmed this rationalization for an ever-increasing number of such systems.[98]

The electrostatic potential of I_3^- is negative on its entire surface but more negative in regions orthogonal to the main axis of the ion and least negative at two caps located on the external iodine atoms and along the main axis (Fig. 5A). This implies that the electrostatic repulsion in $I_3^-\cdots I_3^-$ adducts is minimized when the region orthogonal to the ion main axis of one I_3^- anion approaches the cap of the external iodine of the other I_3^- anion. Indeed, in several structures of the CSD, nearby triiodide units adopt an orthogonal orientation and dimers[100] or infinite chains[101] can be formed (Fig. 5B and D).

Interestingly, NCIplot analysis reveals that a green isosurface is found between the interacting iodine atoms, namely, the HaB observed in the crystal is attractive, and this is also the case when the two anions adopt a binding geometry quite different from the preferred orthogonal arrangement described above.[102]

An anisotropic distribution of electron density is also present in polyiodides wherein two or three iodine molecules are bonded to a central iodide, namely, in the V shaped I_5^- anion and in the I_7^- anion adopting a trigonal pyramidal geometry. In
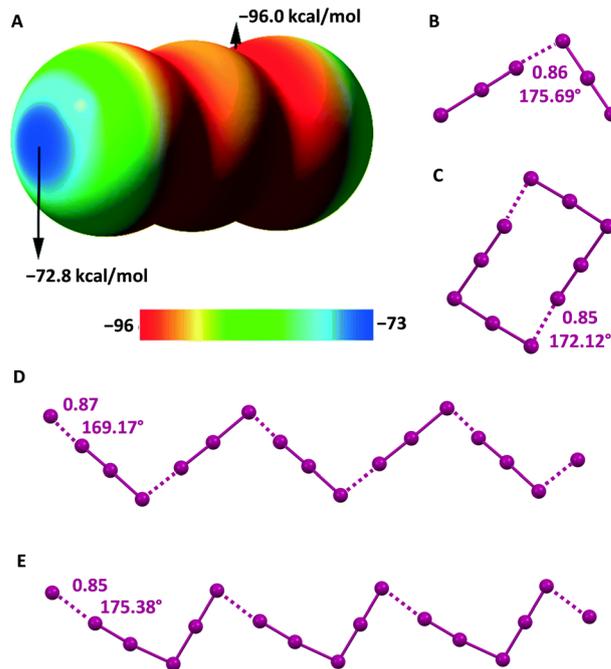

Fig. 5 MEP surface of I_3^- using the 0.001 au isosurface (calculated at the M06-2X/def2-TXVP level of theory) (A).[102] Ball and stick representation of: $I_3^-\cdots I_3^-$ dimers in an L-tyrosinium salt (Refcode ILUSUF)[100] (B) and the $I_3^-\cdots I_3^-$ infinite chain in the salt of a (tetrathiacyclotetradecane)–palladium(II) derivative (Refcode UHANUM)[101] (D); $I_5^-\cdots I_5^-$ dimers in the salt of the radical cation of a tetrathiafulvalene derivative (Refcode CUTXUN)[103] (C) and the $I_5^-\cdots I_5^-$ infinite chain in 4-(pyrimidin-2(1H)-ylidenesulfamoyl)anilinium pentaiodide (Refcode JUPDEF)[107] (E). Cations have been omitted for the sake of clarity; HaBs are violet dotted lines; HaB angles and Nc values are reported close to the interactions.

these anions, a higher and lower electron density is present orthogonal to the I–I covalent bonds and at the cap of the external iodine atoms opposite to these bonds. Consequently, I_5^- and I_7^- anions self-assemble into adducts preferentially adopting an orthogonal binding geometry similar to that described above for the I_3^- anion. Discrete supramolecular polyanions,[103,104] infinite chains,[105–107] (Fig. 5C and E) or even more complex topologies[108] (Fig. 6) are formed. The convenient design of the cation enables the templating of the structure of the obtained polyhalide through a tailored combination of geometric and electronic features. This is the case, for instance, for the dianions $X^-\cdots I_2\cdots X^-$, (X = I,[106,109–113] Br,[106,111] and Cl[59,106,111]) and for the trianion[114] $I^-\cdots I_2\cdots I^-\cdots I_2\cdots I^-$ (Fig. 7).

The tendency of different halogen atoms to form HaBs decreases in the order I > Br > Cl > F and the number of CSD structures containing polyhalide anions decreases in the same order but the preferred arrangement of bonded units remains as described above.[115] The Br_3^- anion shows an anisotropic distribution of the electron density similar to that of the I_3^- anion and its HaB driven assembly into polyanionic supramolecular adducts occurs adopting analogous orthogonal arrangements of interacting units (Fig. 8).[116]

In the CSD, crystalline solids can be found wherein the $O_4I^-\cdots IO_4^-$ supramolecular synthon drives the formation of

This journal is © The Royal Society of Chemistry 2024

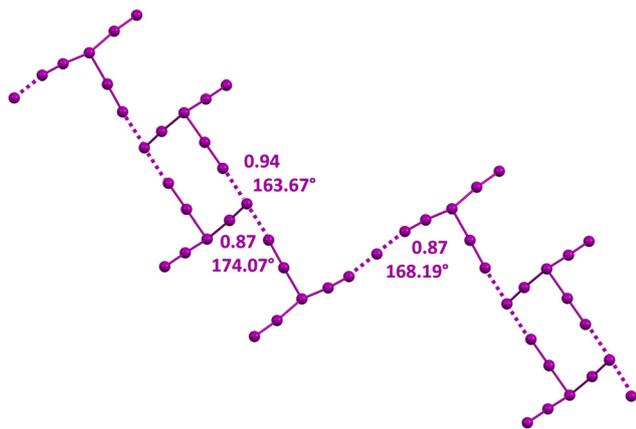*Chem. Soc. Rev.*, 2024, **53**, 6654–6674 | **6661**

Fig. 6 Ball and stick representation of the infinite chain with pendants assembled *via* HaBs involving I^- and I_7^- anions in a salt of the tetrakis(10*H*)-phenothiazin-10-ium radical cation (Refcode EWEKUP).[108] Cations have been omitted for the sake of clarity; HaBs are violet dotted lines; HaB angles and Nc values are reported close to the interactions.
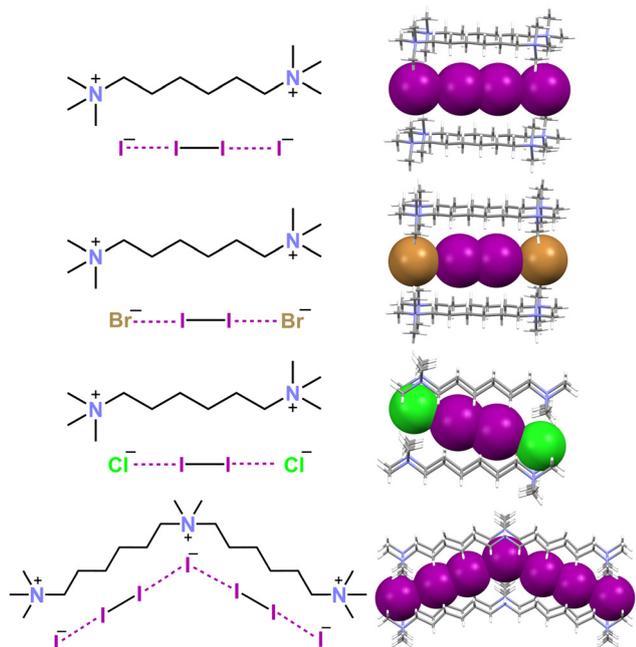

Fig. 7 Structural formulas and partial representation of the crystal packing of the dianions $X^-\cdots I_2\cdots X^-$ (X = I, Br, and Cl) in respective decamethonium salts (Refcodes NUTSOL, DIQBOW, and DIQBUC),[109,111] and the trianion $I^-\cdots I_2\cdots I^-\cdots I_2\cdots I^-$ in the N,*N*,*N*,*N*′,*N*′-pentamethyl-*N*′-(6-(trimethylammonio)hexyl)hexane-1,6-diaminium salt (Refcode PEKKEX).[114] Cationic units are depicted as sticks and the anionic ones are shown in space filling representation. Colour code: grey, carbon; indigo, nitrogen; violet, iodine; green, chlorine; and ocher, bromine.

Fig. 8 MEP of Br_3^- using the 0.001 a.u. isosurface (left).[115] Ball and stick representation of the $Br_3^-\cdots Br_3^-$ adduct in the crystal of the tribromide of a tetrahydropyrrolo[2′,3′:3,4]pyrrolo[1,2-*a*](benzimidazole-1,10-diium) derivative (Refcode IYEVAL) (right).[116] Cations have been omitted for the sake of clarity; HaBs are ocher dotted lines; HaB angles and Nc values are reported close to the interaction.

density on the anion. Moving from this hypothesis some pyridinium periodates (wherein the cation could act as an effective HB donor) were prepared. The single crystal X-ray analyses of these salts confirmed the presence of short HBs and of $O_4I^-\cdots IO_4^-$ adducts assembled *via* different patterns of HaBs.[119] For instance, in two crystals, dimers were present where the two anions were coupled through the antiparallel pairing of the I–O moieties of different IO_4^- units (Fig. 9, bottom).

The MEP of the naked periodate anion is negative on the whole surface but the anisotropic distribution of the electron density generates four symmetric and negative σ-holes on the extension of the four O–I bonds. Differently, the MEP of a pyridinium periodate ion pair in the geometry adopted in the
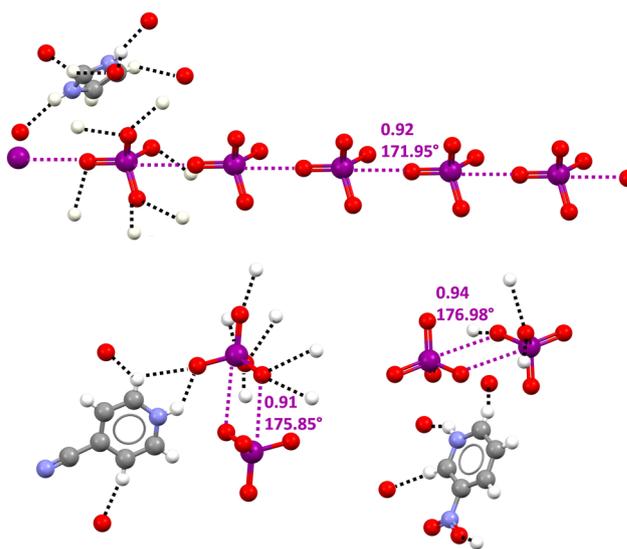
Fig. 9 Ball and stick representation of an anionic supramolecular chain assembled *via* $O_4I^-\cdots IO_4^-$ HaBs in imidazolium periodate (Refcode JOJYOY)[117] (top) and $O_4I^-\cdots IO_4^-$ dimers assembled *via* the antiparallel pairing of two O–I bonds in 4-cyanopyridinium and 3-nitropyridinium periodates (Refcodes BEKNIS and BEKNOY)[119] (bottom). One cationic unit is reported for each structure and the HBs involving this cation and one anionic unit are given (black dotted lines); HaBs are shown in violet dotted lines; HaB angles and Nc values are reported close to the interactions. Colour code: whitish, hydrogen; grey, carbon; red, oxygen; indigo, nitrogen; and violet, iodine.

infinite chains[117] or discrete adducts[118,119] (Fig. 9). In these structures oxygen atoms of periodate anions typically act as donors of electron density in quite short HBs with hydrogen atoms of the cation and this may contribute to unmasking the HaB donor potential of iodine atoms by decreasing the electron
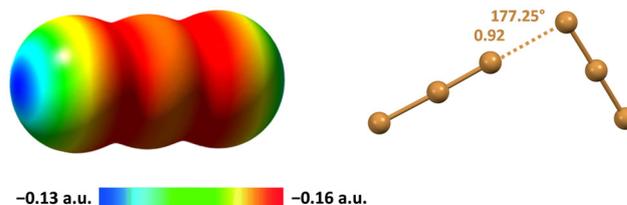
6662 | *Chem. Soc. Rev.*, 2024, **53**, 6654–6674

This journal is © The Royal Society of Chemistry 2024
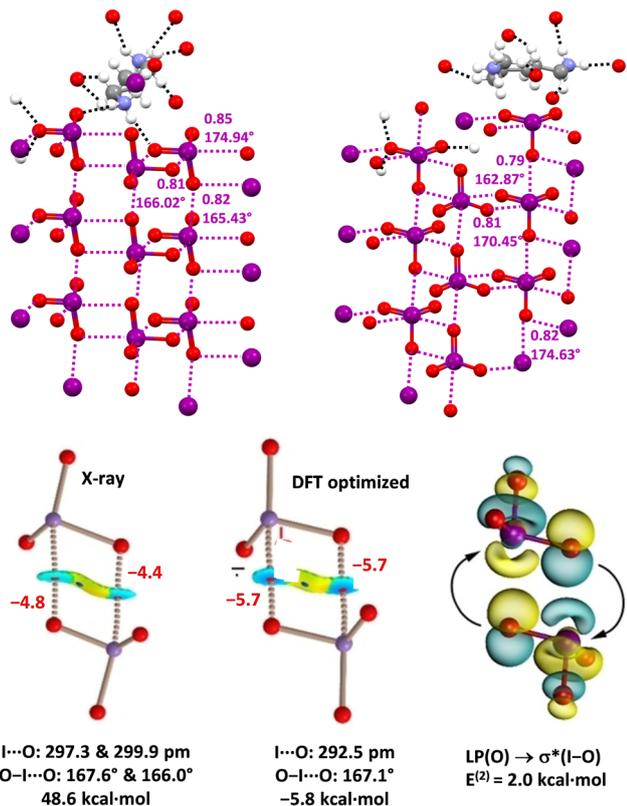
Fig. 10 Crystal packing (ball and stick representation) of iodates of 1,4-diammonium-butane (Refcode VITFEN)[24] (top, left) and 1,6-diammonium-hexane (Refcode VITFIR)[24] (top, right); one cationic unit for each salt and the HBs (black dotted lines) involving this cation and one anionic unit are reported; HaBs are shown in violet dotted lines; HaB angles and Nc values are given close to the interactions. Colour code: whitish, hydrogen; grey, carbon; red, oxygen; indigo, nitrogen; and violet, iodine. QTAIM/NCIPlot analyses of the anion···anion dimer in 1,4-diammonium butane iodate with X-ray geometries and in the gas phase (bottom, left) and with optimized geometries with a continuum solvation model in water (bottom, mid); geometric features and interaction energies are shown in black; HaBs energies (kcal mol^{-1}) are shown in red. NBO characterization of LP(O) → σ*(I–O) interactions via analysis for the anion···anion optimized dimer (bottom. right); $E^{(2)}$ energy is shown in black.

corresponding crystal shows that the electrostatic potential at the σ-holes becomes positive so that also the electrostatic

component of the O–I···O HaBs observes in the crystals may act as a stabilizing force. The attractive nature of these short O–I···O contacts was confirmed by the bond path, bond CPs, and bluish RDG isosurfaces identified by QTAIM/NCIPlot analyses.

CSD analyses reveal that the iodine atom in iodate anions can function as a remarkably effective HaB donor as it can act as a mono-, bi-, and tridentate HaB donor and assemble one,[120] two[24] and three[121] dimensional supramolecular polyanions (Fig. 10, top). Also, bromine in bromate anions can function as a HaB donor[24,122] and not surprisingly it seems to be a weaker donor than iodine in iodate anions. In these systems, QTAIM/NCIPlot analyses identified the presence of bond paths, bond CPs, and blue RDG isosurfaces in each O–I/Br···O contact. The interaction energies for the dimers in X-ray geometry are positive (repulsive) in the gas phase, but they become negative (attractive) in water solution. The natural bond orbital (NBO) methodology confirms the σ-hole nature of the O–I···O contacts identifying the orbital donor–acceptor component (LP(O) → σ*(I–O)) (Fig. 10, bottom).

The HaB driven self-assembly of halocarbon anions into anion···anion adducts[15] has been studied and identified in the solid state via single crystal X-ray analyses,[64,123] in solution via UV-vis[67,123] and modelling,[57,63] and in the gas phase via modelling.[57,62,63] The molecular structures of the used iodocarbon anions are quite different including halo-alkanes, -alkenes, -alkynes, and -arenes; some structures are reported in Table 1 and Scheme 2 while some others are shown in Scheme 4. As expected, the stability of the adducts decreases in the order C–I > C–Br > C–Cl.[57,62] Some of the observed HaBs are quite short (e.g., Nc = 0.80)[64] and strong (e.g. $\Delta E_{int.,water}$ = −5.6 kcal mol^{-1}),[63] probably due to the non-minor geometric and electronic separation of the halogen and the atom(s) where the anion negative charge is mainly localized.

3.2. σ–Hole interactions at d block elements

Initial studies on σ–hole interactions focused on systems wherein the electrophilic atom was a p block element. In 2014, it was first anticipated that d block elements could also act as the electrophile in this type of interactions.[124] The first papers confirming this possibility appeared in 2017[125] when it was described that the catalytic abilities of gold nanoparticles is
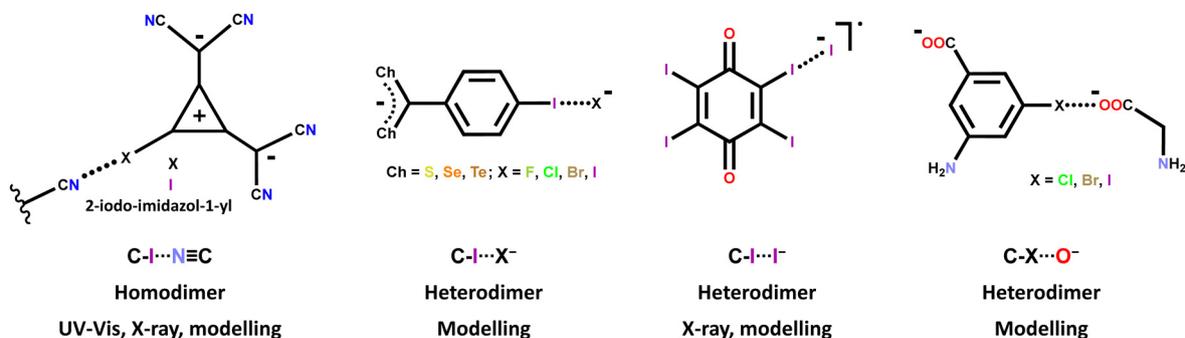
Scheme 4 Structural formulas of some halocarbons forming halogen bonded anion···anion adducts. The interaction and adduct features and the used analytical techniques are also given.

This journal is © The Royal Society of Chemistry 2024

Chem. Soc. Rev., 2024, **53**, 6654–6674 | **6663**

related to the presence of σ-holes at their surface and that these holes serve as binding sites for Lewis bases.

CSD structures wherein d block elements form anion···anion adducts by acting as electrophiles and forming short contacts with geometric and electronic features typical for σ–hole interactions were reported as early as the nineteen seventies[126] but, to the best of our knowledge, the rationalization of these interactions within the framework of σ–hole bonds was first published in 2021[25] when O_4Ma^-··· O_4Ma^- adducts (Ma = Re, Tc, and Mn) were obtained by design and their characteristics were thoroughly studied. The term matere bond (MaB) has been proposed to name these σ–hole interactions wherein the electrophile is an element of group 7. Similar to what is observed for the elements of other groups of the periodic table, the tendency of group 7 elements to act as electrophiles in MaO_4^- anions and to form anion···anion complexes, increases with their atomic weight.[25] In crystals, two adjacent MaO_4^- anions can interact with each other through a singly pinning supramolecular synthon (i.e., through the approach of the O of one anion to the metal of the nearby anion) and supramolecular anionic dimers[25,127,128] or infinite chains[25,129–131] are formed (Fig. 11A and B). Alternatively, two adjacent MaO_4^- anions can be bonded to each other through a doubly pinning supramolecular synthon (i.e., though the antiparallel pairing of the Ma–O moieties of one anion with the Ma–O moieties of a nearby anion). Most frequently, the group 7 elements function as monodentate donors of MaB, and in such cases, the doubly pinning synthons affords dimers[25,60,129,132,133] (Fig. 11D). But occasionally rhenium can also act as a bidentate donor of MaB and in this case discrete adducts[134] and 1D or 2D[60,134–136] networks are formed wherein the singly pinning synthon can also be present (Fig. 11C, E and F). Interestingly, two rhenium atoms in the polyoxorhenate(VII) dianion $Re_4O_{15}^{2-}$ can act as MaB donors and form a ribbon with a nice structure (Fig. 11G).[130]

Experimental techniques (single crystal X-ray analysis, 135/137 NMR and NQR spectroscopy)[25,60,129–132,137] and computation (MEP surface, QTAIM/NCIPlot, and Hirshfeld surface analyses)[25,60,129,130,133] consistently prove the σ-hole character and the attractive nature of the short contacts observed in the crystals. In isolated MaO_4^- anions there are four identical σ-holes where the electrostatic potential is negative but less negative than in other regions. In anion–cation pairs, the holes are no more identical and, more importantly, their potential increases and becomes positive in TcO_4^- and ReO_4^- (Fig. 2). Bond paths and bond CPs have been found for these interactions and NCIPlot analyses revealed extended green/blue surfaces.[25,129]

Tetrachloro-nitrido-technetate anions adopt a square pyramidal geometry and afford matere bonded infinite chains[129,138] via the approach of the nitrogen to the σ-hole at technetium opposite to the Tc≡N bond (Fig. 12).

Some CSD structures containing chromate, bichromate, and trichromate dianions (CrO_4^{2-}, $Cr_2O_7^{2-}$, and $Cr_3O_{10}^{2-}$, respectively) form discrete adducts, chains,[139] ribbons,[140] and 2D networks[126] via short and almost linear O–Cr···O contacts
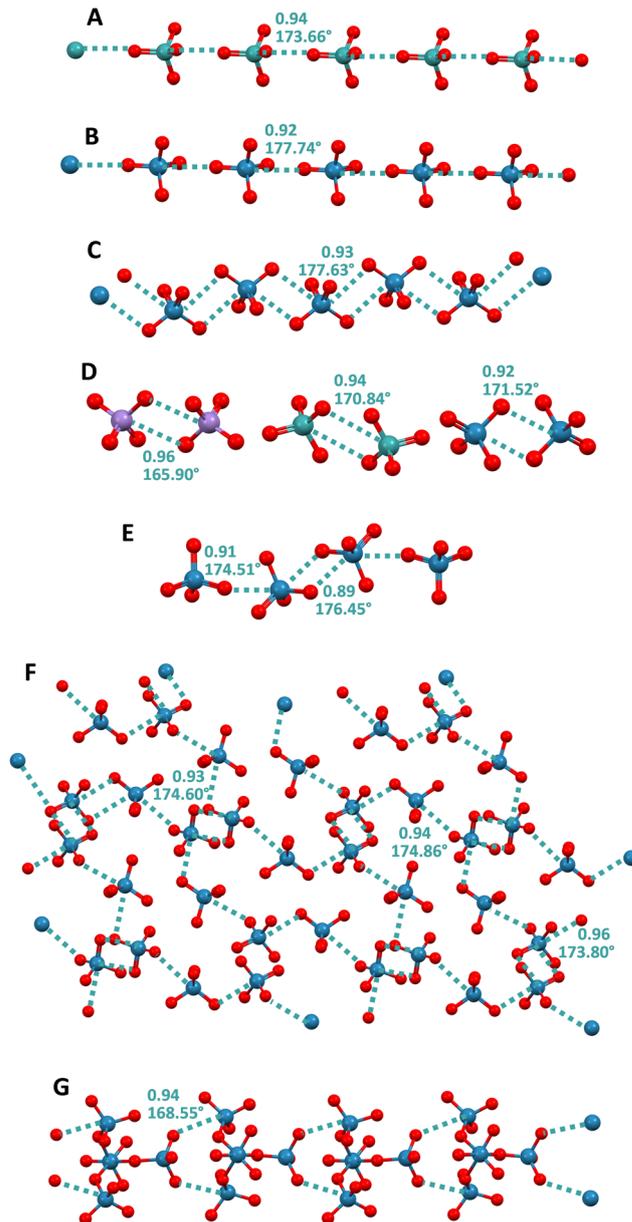
Fig. 11 Ball and stick representation of infinite chains formed by TcO_4^- in its pyrazolium salt (Refcode VISXII)[130] (A) and ReO_4^- in its melaminium salt (Refcode NAPVUZ)[25] (B) and in a $Rh^{2+/3+}$ salt (Refcode DELZUQ)[135] (C); dimers of MnO_4^- in melaminium salt (Refcode NAPWAG)[25] (D, left) and of TcO_4^- and ReO_4^- in guanidinium salts (Refcodes GEQHUJ and GEQJAR)[60] (C, mid and right); tetramer of ReO_4^- in its salt with a pyridinium derivative (Refcode ZUYKAH)[134] (E); 2D net of ReO_4^- in a salt with protonated N-methyl-DABCO (Refcode FAWDEQ)[136] (F); ribbon of $Re_4O_{15}^{2-}$ in a pyrazolium salt (Refcode VISXAA)[130] (G). Cations have been omitted for clarity; MaBs are teal dotted lines. Colour code: red, oxygen; lavender indigo, manganese; teal, technetium; and imperial blue, rhenium.

between adjacent anions. These anion···anion interactions have the geometric and electronic features[141] for being rationalized as wolfium bonds (WfBs),[142] which are σ-hole bonds wherein an element of group 6 of the periodic table interacts with an electron donor.

6664 | Chem. Soc. Rev., 2024, 53, 6654–6674

This journal is © The Royal Society of Chemistry 2024

Similarly, some orthovanadate anions, specifically the monoanions of orthovanadate diesters $(RO)_2VO_2^-$, form dimers[143] and infinite chains[144] *via* short and almost linear O–V⋯O contacts between nearby anions. These anion⋯anion interactions can be considered erythronium bonds (EyB),[145] the σ-hole interaction wherein an element of group 5 is the electrophile.
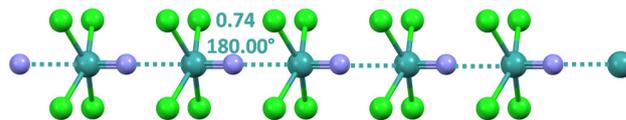

Fig. 12 Ball and stick representation of the infinite chain formed by the tetrachloro-nitrido-technetate anion (Refcode SODWIR10).[138] Cations have been omitted; MaBs are shown in teal dotted lines. MaB angles and Nc values are reported close to the interaction. Colour code: green, chlorine; indigo, nitrogen; and teal, technetium.

4. Adducts assembled by π-hole interactions

4.1. π-Hole interactions at s- and p-block elements

Computation shows that in the dihalides of alkali metals $(AX_2^-$, A = Li and Na; X = F and Cl) adopting a linear geometry, the less negative (most positive) region is a belt around the alkali metal atom and orthogonal to the main axis of the anion. The approach of a halide anion to this region results in the formation of $X_2A^-\cdots X^-$ dianion systems whose optimized structure exhibits minima with trigonal geometry (D_{3h} symmetry).[146] The formation of $X_2A^-\cdots X^-$ dianions through binding of the X^- and AX_2^- monoanions is endothermic for all examined systems, but these dianions are kinetically stable as their spontaneous dissociation is prevented by a maximum that is present along the dissociation profile. QTAIM analyses reveal that a bond CP is present in the three metal–halogen bonds of all dianion adducts.

CSD analyses show that in the solid state, the dihalides of some alkaline earth metals can form tetrahalide dianions that typically adopt a tetrahedral geometry (*e.g.*, AeX_4^{2-}, Ae = Be and Mg; X = F, Cl, and Br).[147–149] Computational studies on $X_3Ae^-\cdots X^-$ and $X_3Ae^-\cdots CN^-$ systems (Ae = Be, Mg, Ca, Sr, and Ba; X = F and Cl)[65,146] have been performed, yielding analogous results for all systems, and these studies support the rationalization of these dianions as stable π-hole species in the solid state. The following discussion concentrates on $AeX_3(CN)^{2-}$ complexes. The $AeCl_3^-$ monoanions all adopt a planar trigonal geometry with D_{3h} symmetry in the gas phase. In aqueous solution, this is the case for the two lighter alkaline earth metal anions while the three heavier ones exhibit a distorted trigonal pyramidal geometry. For $BeCl_3^-$ and $MgCl_3^-$, the electrostatic potential is negative on the whole surface, but less negative at the π-holes above and below the metal atom. In $CaCl_3^-$, $SrCl_3^-$, and $BaCl_3^-$, the potential distribution is similar in shape to that of the lighter anions, but the numerical value at the π-hole is positive. On approaching one of these holes, the CN^- anion promotes the pyramidalization around the metal centre. Importantly, in pyramidal $AeCl_3^-$ the potential in the hole region becomes positive for all the five anions; in this geometry monoanions are ready to form an attractive electrostatic interaction with the incoming CN^- anion. The $X_3Ae^-\cdots CN^-$ dianions are metastable species in the gas phase, requiring an energy barrier of approximately 20 kcal mol^{-1} to overcome in order to transform into the more stable separated monoanions (Table 3). In water these barriers disappear and

Table 3 Binding energies (E_b, kcal mol^{-1}) of $AeCl_3CN^{2-}$ dianions calculated at the MP2/aug-cc-pVDZ (MP) and CCSD(T)/aug-cc-pVDZ (CCDC) levels in the gas phase and in aqueous solution. All values are corrected for BSSE
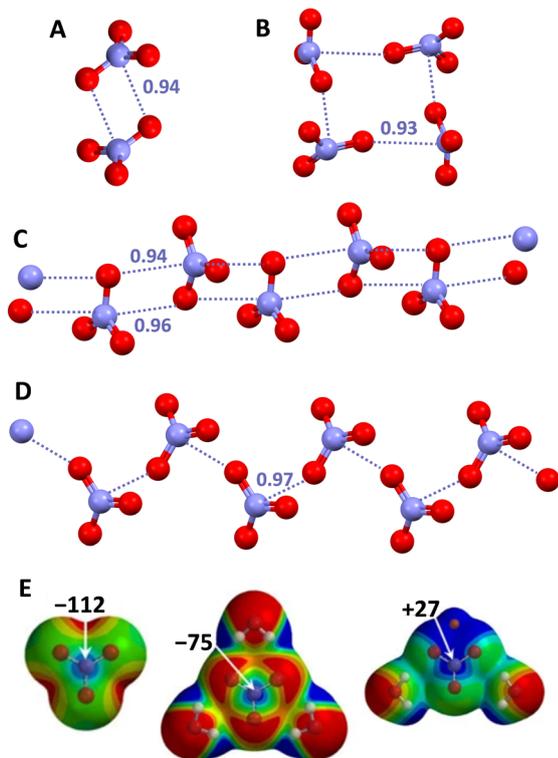
Complex	$E_{b(gas\ phase)}$		$E_{b(water\ sol.)}$	
	MP	CCSD	MP	CCSD
$Cl_3Be^-\cdots NC^-$	42.76	44.49	−19.55	−17.56
$Cl_3Mg^-\cdots CN^-$	27.70	27.85	−15.75	−15.61
$Cl_3Ca^-\cdots CN^-$	20.31	20.20	−7.80	−7.83
$Cl_3Sr^-\cdots CN^-$	19.30	18.97	−5.47	−5.44
$Cl_3Ba^-\cdots CN^-$	15.76	15.23	−1.24	−1.20

the dianions become thermodynamically more stable than the two separated monoanions.

The case of nitrate anions (NO_3^-) is particularly important due to the common presence of this anion in both synthetic and natural systems. Already in 2006, the formation of nitrate⋯nitrate dimers was recognized as a structure determining factor in a crystalline aminoguanidine salt.[150] One year later, a CSD analysis proved that $O_3N^-\cdots O_3N^-$ interactions are relatively common in crystalline solids and can play a non-minor role in determining the structure of the corresponding salts.[151] Adjacent anions can interact with each other either *via* a singly pinning supramolecular synthon (wherein the O of one NO_3^- unit approaches the N atom of a nearby NO_3^- unit forming O–N⋯O angles close to 90°) or *via* a doubly pinning supramolecular synthon (wherein there is the antiparallel pairing of the N–O moieties of two nitrate anions, once again the O–N⋯O angles being close to 90°). Anionic adducts with different topologies (*e.g.*, either discrete systems such as dimers,[150,151] trimers,[152] and tetramers[153,154] or infinite chains[155,156]) are formed thanks to the presence of one or both supramolecular synthons (Fig. 13).

This behaviour is consistent with the anisotropic distribution of charge in NO_3^-. Above the nitrogen atom there is a π-hole which is remarkably negative in the naked anion but is substantially dampened if water molecules are close to the oxygen atoms and becomes positive in the neutral species $LiNO_3\cdot2H_2O$ (Fig. 13, bottom).[157] Interestingly, the single crystal study of urea nitrate, a high explosive, showed the presence of nitrate dimers assembled *via* doubly pinning supramolecular synthons. The topological analysis of the distribution of electron density in this salt, revealed that the observed N⋯O PnBs are not solely driven by the tight network of cation⋯anion
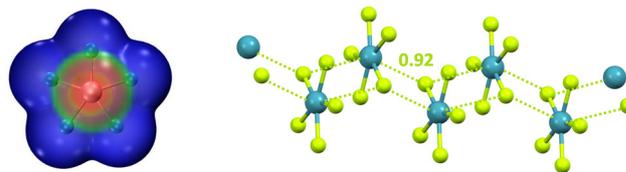
This journal is © The Royal Society of Chemistry 2024

Chem. Soc. Rev., 2024, **53**, 6654–6674 | **6665**

Fig. 13 Ball and stick representation of supramolecular anionic adducts formed by NO_3^-: dimer in an aminoguanidine salt (Refcode GEMMUH)[150] (A); cyclic tetramer in a Pt(II) organometallic complex (Refcode EWIDIY)[153] (B); infinite chains assembled via singly (Refcode JUMSOR)[156] (C) and doubly (Refcode EDOHOU)[155] (D) pinning supramolecular synthons in a copper(II) coordination complex and in the triethylenetetra-ammonium salt, respectively; cations have been omitted for clarity; PnBs are shown with indigo dotted lines. Nc values of PnBs are reported close to the interactions. Colour code: red, oxygen and indigo, nitrogen. MEP of naked (E, left) or trihydrated (E, mid) NO_3^-, and of $LiNO_3 \cdot 2H_2O$ (E, right) obtained at the MP2/6-311pG** level (energy values in kcal mol^{-1}); colour scale ranges from more negative (red) to more positive (blue) potentials in between −155 and −122 (E, left), −102 and −75 (E, mid), and −48 and −27 (E, right).[157]

Fig. 14 Left: MEP of naked XeF_5^- (obtained at the MP2/aug-cc-pVDZ level of theory); colour scale ranges from −0.13 (blue) to −0.11 (red) a.u.[27] Right: ball and stick representation of the infinite chains formed by XeF_5^- in its tetramethylammonium salt (Refcode SOBWAH);[158] cations have been omitted for clarity; NgBs are represented by acid yellow dotted lines; Nc value of NgB is reported close to the interaction; colour code: light teal xenon and acid yellow, fluorine.
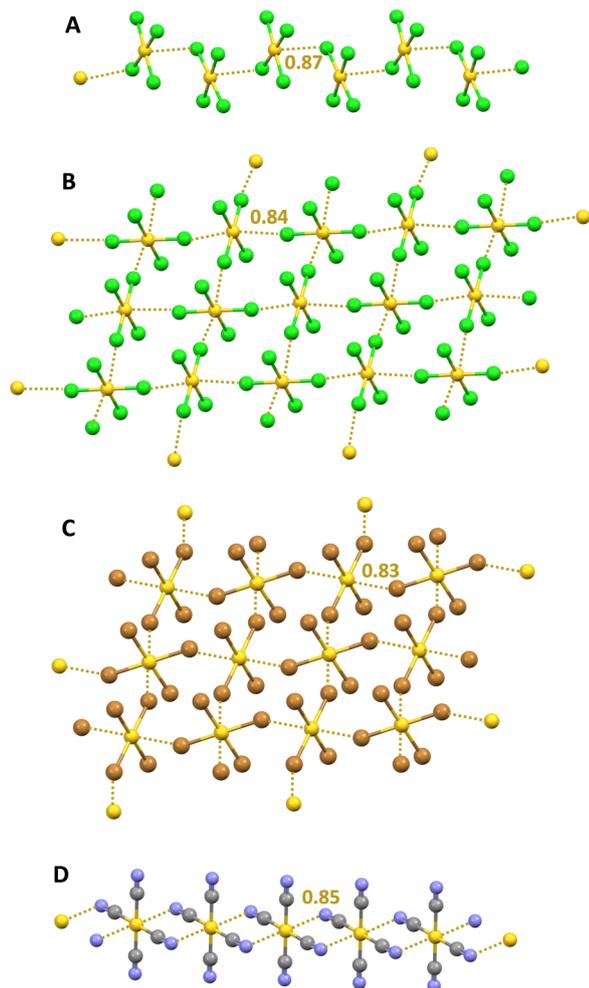
The ability of π-hole interactions to drive the self-assembly of as exotic systems as XeF_5^- forcefully confirms how general and reliable the possibility to direct anion···anion assembly via σ/π-hole interactions is.

4.2. π-Hole interactions at d-block elements

The tetrachloridopalladate and tetrabromidopalladate anions (PdX_4^{2-}, X = Cl and Br) adopt in the solid a square planar geometry. Salts wherein these anions are paired with cations that can form a tight network of H···X HBs (e.g., α,ω-diammoniumalkanes) can occasionally show the presence, in the solid, of anions dimers[159] and trimers[28,160] which are assembled via Pd···X short contacts wherein the halogen of one unit approaches the palladium of another unit orthogonal to the plane of this second unit. A computational study[28] rationalizes these contacts as π-hole interactions. In fact the MEP of the anion reveals two regions of less negative electrostatic potential above and below the metal and QTAIM/NCIPlot analyses identify a bond path connecting palladium and halogen atoms as well as a bond CP and a green disk along the path. The NBO analyses detect a halogen → metal charge transfer associated with the overlap of a halogen lone pair with a vacant Rydberg orbital on palladium.

A similar ability of $AuCl_4^-$ anions to self-assemble into supramolecular anionic chains in the solid via short Au···Cl contacts was first reported nearly fifty years ago.[161] Various other studies have subsequently acknowledged the propensity of AuX_4^- anions (X = Cl and Br) to self-assemble into discrete adducts or infinite networks,[162,163] either through a singly pinning supramolecular synthon (in which the halogen of one unit gets close to the gold atom of another unit and the X–Au···X angle is close to 90°), or through a doubly pinning supramolecular synthon[164] (in which the Au–X moiety of one anion couples with the Au–X moiety of a nearby anion after an antiparallel orientation and a nearly orthogonal geometry) (Fig. 15A–C). The tetracyanido anion $Au(CN)_4^-$ shows a similar interactional landscape forming discrete adducts and 1D[165] or 2D networks[166] via orthogonal C–Au···N short contacts (Fig. 15D). Recently, these interactions have been rationalized as coinage bonds (CiBs), namely the interactions wherein an element of the group 11 acts as an electrophile and attractively interacts with a donor of electron density (nucleophile). The

interactions but also result from the electrostatic nature of the interaction between the like-charged moieties.[151]

After discussing anion···anion adducts assembled through π-hole interactions wherein the electrophilic atom is an element of groups 1, 2, or 15, we consider adducts formed by the noble gas bond (NgB), the interaction wherein the element hosting the hole belongs to group 18.[27] Calculations predict that NgX_5^- (Ng = Kr and Xe; X = F and Cl) are planar systems with approximate D_{5h} symmetry. Above and below the noble gas atom, the surface electrostatic potential presents regions (π-hole) where the electrostatic potential is the least negative (Fig. 14, left) and these are the regions of preferential approach of anions such as F$^-$, Cl$^-$, and CN$^-$. The formed supramolecular dianions are stable in polar media (e.g., aqueous solution) and metastable in less polar environments (e.g., THF and DMF solvents). The anionic infinite chain present in crystalline $NMe_4^+XeF_5^-$ (Fig. 14, right) confirms the theoretical results.[158]

6666 | Chem. Soc. Rev., 2024, 53, 6654–6674

This journal is © The Royal Society of Chemistry 2024

Fig. 15 Ball and stick representation of supramolecular anionic: 1D networks formed by AuCl$_4^-$ in its *S*-benzyl-isothiouronium salt (Refcode BTURAN)[161] (A) and by AuCN$_4^-$ in an (ethylenedithio)(diselenadithiafulvalene) salt (Refcode XIZCOY);[166] 2D networks formed by AuCl$_4^-$ in its pyrazinium salt (Refcode BIHXIC)[162] (B) and by AuBr$_4^-$ in its methylammonium salt (Refcode LONBUO)[163] (C); cations have been omitted for clarity; CiBs are shown in ocher dotted lines. Nc values of CiBs are reported close to the interactions. Colour code: yellow, gold; green, chlorine; ocher, bromine; grey, carbon; and indigo, nitrogen.

MEP analyses of AuCl$_4^-$ shows the presence of two regions above and below the gold atom where the electrostatic potential is maximum (π-holes) in both the isolated anion and in cation–anion pairs.[26] The value of the potential is negative using the 0.001 a.u. isovalue but becomes positive for the ion pair when the 0.008 a.u. isovalue is used (Fig. 1). The QTAIM/NCIPlot analyses of Cl–Au···Cl contacts in the geometries observed in the crystals reveal the presence of a bond CP and a bond path connecting the gold and chlorine atoms, indicating that the anion···anion interactions between AuCl$_4^-$ units serve as robust and reliable supramolecular synthons for the control of the overall packing in crystalline structures. Similar computational results were obtained for the anion···anion interactions between Au(CN)$_4^-$ and several different mono- and polyatomic anions.[167] For instance, the dimers with fluoride,

chloride, cyanide, and hypochlorite anions are metastable species characterized by potential wells. The electron withdrawing ability of the CN$^-$ residues in Au(CN)$_4^-$ units and the small size of the anion approaching the gold atom seem to be two critical aspects for the existence of these metastable dianions. QTAIM analysis of the interaction between gold and the incoming anion shows a bond CP with appropriate electron density and positive Laplace values, as typical for close–shell interactions.

In the CSD, the trihalides of the group 12 elements SpX$_3^-$ (Sp = Zn, Cd, and Hg; X = Cl, Br, and I) can exist as isolated units adopting a trigonal and nearly planar geometry or as dimeric, oligomeric, and polymeric adducts wherein one or two halogen atoms bridge adjacent metal centres. The structural diversity of the anion complexes present in the CSD is attributed to the different geometries around the metal and the diverse nature of the metal–halogen bonds. In many crystalline systems, anion adducts show a deformed tetrahedral arrangement around the metal which forms four short and nearly equivalent Sp–X bonds characterized by a strong covalent nature.[168] Calculations indicate that these systems can be rationalized as covalently bonded adducts which are stable in the vacuum, ethanol, and water environment. In a smaller number of adducts, the SpX$_3^-$ units largely retain their native planar D_{3h} geometry and are held together by noncovalent Sp···X interactions which can be rationalized as π-hole spodium bonds (SpBs), the interactions wherein the group 12 element acts as the electrophilic site.[169] The Sp···X interactions are much longer than the other three Sp–X bonds forming the SpX$_3^-$ units. Also these discrete or infinite supramolecular systems[170,171] (Fig. 16) wherein SpX$_3^-$ units are connected by longer and non-covalent bonds, can be assembled via singly or doubly pinning supramolecular synthons, analogous to those described above for AuX$_4^-$. As expected, calculations show that the spodium bonded adducts are not a stable minimum in the gas phase, but they do exist in ethanol and water solution and for systems involving Hg, the heaviest element of the group, they are more stable than the corresponding covalent anion complexes. Analysis of the electron density topology in Hg···Cl interactions of HgCl$_3^-$ homodimers revealed a bond path between the mercury and chlorine atoms and a density at the critical point having the characteristic value of noncovalent interactions of reasonable strength.[172] A green RDG isosurface characterizes these interactions so that their attractive nature is confirmed, notwithstanding the Coulombic repulsion between the two anions. Similarly, CN$^-$ and SpCl$_3^-$ form heteromeric dimers that are less stable than the pairs of separated ions in gas phase, but in aqueous solution, the dimerization process is exothermic.[173]

5. Applicative impacts

5.1. Biorelevant systems

PDB analyses show that anion···anion interactions are not exceptional in the protein environment. For instance, 24% of

This journal is © The Royal Society of Chemistry 2024
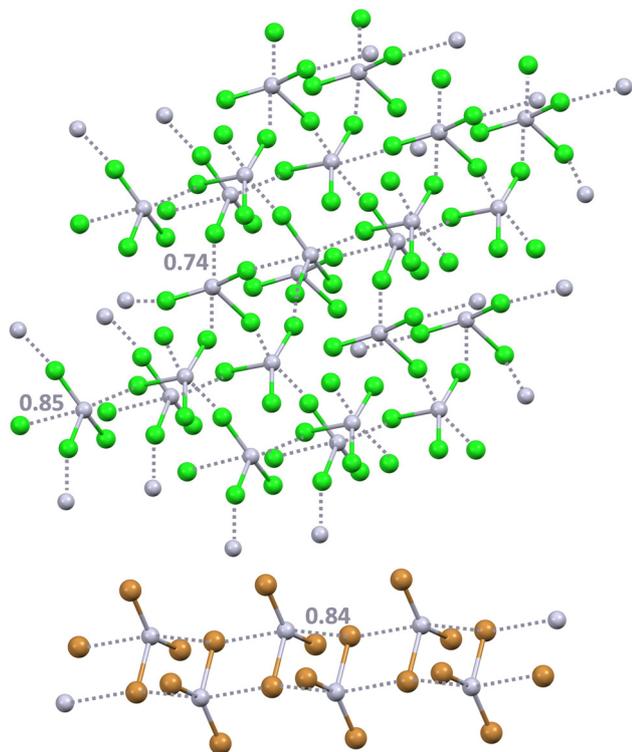
Chem. Soc. Rev., 2024, **53**, 6654–6674 | **6667**

Fig. 16 Ball and stick representation of the supramolecular anionic 3D network formed by HgCl$_3^-$ via SpBs in the methylammonium salts (Refcode QQQBVJ04)[170] (top) and the 1D network formed by HgBr$_3^-$ in the salt with a benzymidazoliun derivative (Refcode WURPOP)[171] (bottom). Cations have been omitted for clarity; SpBs are shown in grey dotted lines. Nc values of SpBs are reported close to the interactions. Colour code: light grey, mercury; green, chlorine; and ocher, bromine.

Fig. 17 Partial view of the complex between a iodipamide fragment and human serum albumin (PDB code 2BXN)[176] evidencing the C–I⋯O HaB between the carboxylate of Asp 451 and the iodocarbon moiety.

the halogenated ligands bonded to a protein and showing structural features consistent with the presence of a HaB are expected to exist as negatively charged species at physiological pH. Quantum mechanics/molecular mechanics studies reveal that the HaBs observed in these crystal structures are stabilizing interactions in the protein environment, while they are unstable or metastable in the vacuum.[66] These interactions may increase the biopharmacological activity of halogenated compounds by increasing their affinity for the target protein pocket.[57] The HaB acceptor is often the oxygen of a backbone amide moiety, although it can also be the oxygen of the carboxylate residue of an aspartic or glutamic acid.[174] For instance, this is the case in the complex between bovine and equine serum albumin and 3,5-diiodosalicilate[175] as well as in the complex between human serum albumin and iodipamide, a well-known contrast agent[176] (Fig. 17).

At physiological pH, ATP and ADP exist as anionic species. According to the associative ATP hydrolysis mechanism, the trigonal–bipyramidal transition state producing ADP and a phosphoric unit involves the attack of an OH$^-$ to the phosphorous of the terminal phosphoric unit of ATP.[18] It may be expected that an anion⋯anion O–P⋯O PnB wherein the OH$^-$ unit is the PnB acceptor and the terminal phosphorous atom of ATP is the PnB donor is en route to the transition state.

Analogously, according to the dissociative ATP synthesis mechanism, it can be expected that an anion⋯anion O–P⋯O PnB wherein an oxygen atom of ADP is the PnB acceptor and a metaphosphate anion is the PnB donor is en route to the formation of ATP from ADP.[20]

At physiological pH, the phosphoric unit also exists in its anionic form and its binding to proteins can be mediated by an anion⋯anion interaction, e.g., when the selectivity versus sulphate anion binding is secured by an HB between a carboxylate residue at the protein active site and the phosphate –OH
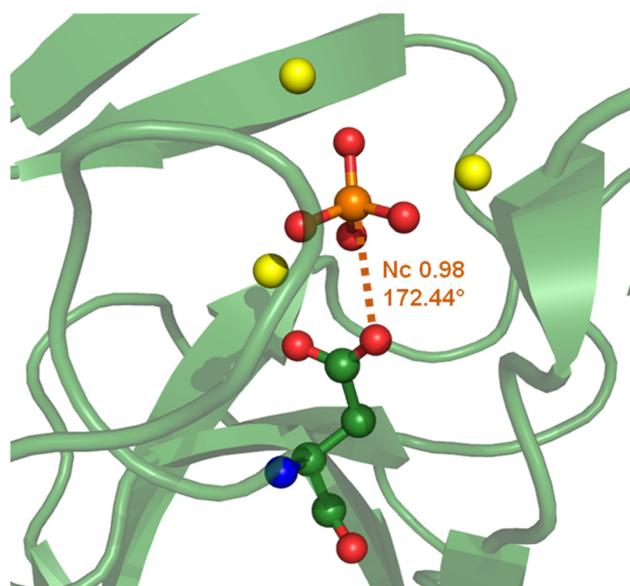
Fig. 18 Partial view of the complex between a phosphoric unit and a hydrolase from *Thermococcus thioreducens* (PDB code 3Q46)[177] evidencing the O–P⋯O PnB between the carboxylate of Asp 71 and the phosphate anion.

6668 | Chem. Soc. Rev., 2024, 53, 6654–6674

This journal is © The Royal Society of Chemistry 2024

group(s).[17] In other cases the anion···anion interaction locking the phosphate within the cavity, can be a O–P···O PnB wherein the PnB donor is phosphate phosphorous and the acceptor is a peptide carboxylate group. For instance, this is the case in the hydrolase enzyme from a thermophilic organism[177] (Fig. 18).

Interestingly, it is known that MgF_4^{2-} dianion acts as a phosphate anion(s) analogue and binds to proteins. At the active site, MgF_4^{2-} can form a short F–Mg···O contact with a carboxylate group of the protein. This anion···anion inter-action can be quite close to linearity and can be rationalized as a σ-hole bond. For instance, such an interaction is found in MgF_4^{2-} bonded to a hydrolase transport protein (sodium/potassium pump)[178] wherein the Mg···O separation corresponds to an Nc value of 0.67 and the F–Mg···O angle is 176.68° (Fig. 19, top). When MgF_4^{2-} binds to a human ATPase, both oxygen atoms of the carboxylate residue of Asp 381 get close to the magnesium, namely, the carboxylate group acts as a bifurcated σ-hole bond acceptor (Fig. 19, bottom).[179] This bifurcated binding mode is well-documented in the literature for σ-hole interactions whenever the acceptor of electron density approaches a moiety having two geminal oxygen atoms.[40]

5.2. Materials

Hybrid organic–inorganic salts are of interest (e.g., when pursuing a variety of electric and photophysical properties) as they enable the exploitation of the functional performances of both organic and inorganic moieties. The overall crystal packing of these systems can be characterized by the segregation of anions into 1D columnar arrangements or 2D layers and this segregation is more likely when anions self-assemble into extended supramolecular adducts.[121] Indeed, hybrid organic–inorganic salts have been reported wherein the structure of the anionic domains is apparently affected or determined by σ/π-hole bonds connecting two or more anions. The strength of these interactions is typically promoted by a network of HBs connecting the organic cations (the HB donors) and the inorganic anions (the HB acceptors) and dissipating the net negative charge of the anions.

Regarding π-hole bonds, gold(III) anions provide an example proving how anion···anion supramolecular architectures assembled by these interactions are not uncommon in useful functional materials. The methylammonium tetrabromidoaurate ($CH_3NH_3^+AuBr_4^-$) and its tetrachlorido analogue form anionic 2D networks assembled via Au···X (X = Cl and Br) CiBs. These Au-based halides show relatively small band gap energies (lower than 2.5 eV) and can be considered as alternatives for Pb-based halides in optoelectronic applications.[163] Anionic 2D nets assembled by Au···Cl π-hole CiBs are also present in pyrazinium tetrachloridoaurate ($C_4H_5N_2^+AuCl_4^-$) and these crystals show a giant 2-dimensional dielectric response.[162] Au···I π-hole CiBs between AuI_4^- and AuI_2^- anions in the mixed-valent gold(I)/gold(III) iodides of α,ω-diammonium alkanes ($[NH_3(CH_2)_nNH_3]_2^{2+}[(Au^II_2)^-(Au^{III}I_4)^-(I_3^-)_2]$ (n = 7, 8)) form 2D networks. These organic-based layered perovskites present an optical band-gap smaller than that of fully inorganic analogous salts.[180] In the tetracyanidoaurate of

a diselenadithiafulvalene, fairly short Au···NC π-hole CiBs assemble the $Au(CN)_4^-$ anions into columnar arrays and the crystals show superconductivity under uniaxial strain.[166]

The anionic 1D and 2D arrays present in crystals endowed with useful functional properties can also be structured under the control of σ-hole bonds. Imidazolium periodate ($C_3H_5N_2^+IO_4^-$) is an improper molecular ferroelectric crystal showing switchable dielectric, piezoelectric, and second-harmonic generation bistability. In its crystals, O–I···O σ-hole HaBs assemble IO_4^- anions into supramolecular chains which segregate into layers.[117]

Analogously, O–Re···O σ-hole MaBs assemble the ReO_4^- anions of some N-ethyl-Dabco perrhenate derivatives (e.g., [N-2-chloroethyl-Dabco$^{2+}(ReO_4)_2^{2-}$]) into supramolecular anionic networks. These hybrid organic–inorganic salts show tunable and switchable dielectric properties.[136] In crystalline 4-aminopyridinium tetrachloroantimony(III) (4-NH$_2$-C$_5$H$_5$N$^+$SbCl$_4^-$), adjacent $SbCl_4^-$ anions are assembled into supramolecular columnar arrangements

Fig. 19 Partial view of the complex between MgF_4^{2-} and a hydrolase transport protein (PDB code 2ZXE)[178] (top) and a human Na$^+$/K$^+$-ATPase (PDB code 8D3X)[179] (bottom) wherein the carboxylate residue of Asp 381 forms an anion···anion σ-hole bond with MgF_4^{2-} acting as monofurcated and bifurcated donors of electron density.

This journal is © The Royal Society of Chemistry 2024

Chem. Soc. Rev., 2024, **53**, 6654–6674 | **6669**

by Cl–Sb···Cl σ-hole PnBs formed through the antiparallel pairing of the Cl–Sb moiety of nearby anions. Below 270 K, these crystals show ferroelectric properties.[181] 1,4-Dimethylpiperazine-1,4-diium tetrachloroantimony(III) chloride $[(C_6H_{16}N_2)]^{2+}[(Sb^{III}Cl_4)^-Cl^-]$ shows enhanced photoluminescent efficiency[87] and Cl–Sb···Cl PnBs are present in its crystals. Specifically, Cl$^-$ anions bridge Sb^{III}Cl$_4^-$ anions and supramolecular anion chains are formed.

6. Summary and outlook

The anion···anion self-assembly is a relatively new entry in the palette of opportunities for controlling the organization of molecular entities in condensed phases. It has become apparent that attractive forces between anions can occur and some of them can be robust enough to overcome the electrostatic repulsion between the net like charge of two anions and to drive their assembly into supramolecular anion···anion adducts.

The σ- and π-hole bonds are attractive noncovalent interactions that occur between nucleophiles and the regions of depleted electron density, which most molecular entities have opposite to their single covalent bonds (σ-holes)[11,12] and perpendicular to their planar regions (π-holes).[13,14] In this review we show that σ- and π-hole bonds wherein anions act as both the nucleophile (via one or more of their regions of high electron density) and the electrophile (via one or more of their σ- and π-holes) can effectively overcome the electrostatic repulsion between the anions and drive their assembly into a variety of structurally different adducts (e.g., discrete dimers or oligomers as well as 1D, 2D, or 3D networks). Typically, these adducts are stable in the solid and in polar solutions and are metastable or unstable in the gas phase.

Regarding the ability of some specific attractive forces between like charges to overcome electrostatic repulsion, it may be useful to summarize that isolated polyatomic anions in their ground state geometry show the presence of σ/π-holes where the electrostatic potential is, in most cases, negative on a surface that is a quite good approximation of the van der Waals surface, namely if the 0.001 a.u. isovalue is used, but occasionally the potential on this surface can also be positive.[65] An incoming and negatively charged nucleophile experiences, at this surface, an electrostatic repulsion in the former cases and an attraction in the latter ones. But the separations in anion···anion interactions considered in this review are shorter than the sum of van der Waals radii of involved atoms and the contribution of the electrostatic forces to the inter-action energy may be better understood by considering surfaces smaller than the van der Waals one, namely, by considering isovalues greater than 0.001 a.u. The electrostatic potential values progressively increase with the isovalue, namely, when getting closer to atoms nuclei, and at interaction distances similar to those observed in anion···anion adducts these values may become positive when they are negative on the 0.001 a.u. isovalue surface.[26] In most cases, the electrostatic force is thus repulsive at long distances and initially increases as anions approach each other, in accordance with the classical Coulomb's law. But, after reaching the Coulombic repulsion barrier, it decreases drastically; at short ranges, the inter-anion electrostatic repulsion among electrons and among nuclei can be overwhelmed by the inter-anion nucleus–electron attractions.[53,89,167]

Anions change their geometry when assembling into adducts and changes tend to be greater when interactions are shorter. These structural rearrangements are invariably endothermic (deformation energies are always positive), but may be favoured by the fact that the electrostatic potential at σ/π-holes of anions adopting the geometry of the adducts is usually more positive (less negative) than when adopting the ground state geometry.[65]

The Pauli exchange repulsion component of the interaction energy is positive (destabilizing) at any interaction distance and becomes greater when the distance decreases. Also the absolute values of charge transfer, dispersion, and polarization energies become greater when the interaction distance decreases, but, differently, they are negative (stabilizing) at any length. The dependence on the interaction distance of all the component energies mentioned above varies from one anion···anion adduct to another, and their combination determines the separation and energy of the interaction.

Cases are described wherein the electrophilic atom of the anion belongs to the 1, 2, 5, 7, and 11–18 groups of the periodic table. Clearly, the electrophilic atom can vary across many groups of the s-, p- or d-blocks, namely the σ/π-hole bonds open the possibility for the self-assembly of a particularly wide diversity of anions. By doing so, σ/π-hole bonds effectively complement the opportunities offered by the HB, probably the most frequently used interaction when the anion···anion self-assembly is pursued.[21,22]

While the field of anion···anion adduct formation under the control of σ/π-hole bonds is possibly leaving its infancy, it may be expected that some anions that can be assembled via these interactions remain to be identified. Other aspects where major advances may occur in the close future are the understanding of the molecular and supramolecular features favouring the anion···anion self-assembly under the control of σ/π-hole bonds (e.g., the most convenient molecular structures of the cations and the overall set of interactions involving the anions). The specific role that σ/π-hole bonds controlling anion···anion self-assembly have in known processes, both chemical and biological, is largely unexplored and expectedly the rational design of anion···anion adducts will offer new and useful opportunities in various fields such as biopharmacology, catalysis, and molecular or polymeric materials.

Conflicts of interest

There are no conflicts to declare.

Acknowledgements

6670 | Chem. Soc. Rev., 2024, 53, 6654–6674

This journal is © The Royal Society of Chemistry 2024

Notes and references

1 G. R. Desiraju, *Angew. Chem., Int. Ed.*, 2007, **46**, 8342–8356.

2 Y. V. Nelyubina, M. Y. Antipin and K. A. Lyssenko, *Russ. Chem. Rev.*, 2010, **79**, 167–187.

3 V. Y. Kotov and S. L. Gorei'sky, *Russ. Chem. Bull.*, 1999, **48**, 823–830.

4 S. R. Kass, *J. Am. Chem. Soc.*, 2005, **127**, 13098–13099.

5 R. Barbas, R. Prohens, A. Bauza, A. Franconetti and A. Frontera, *Chem. Commun.*, 2019, **55**, 115–118.

6 M. O. Miranda, D. J. R. Duarte and I. Alkorta, *ChemPhysChem*, 2020, **21**, 1052–1059.

7 The wording short contact, or close contact, is used for any bonding when the separation between the involved atoms is longer than sum of respective covalent radii but shorter than the sum of van der Waals radii (S. S. Batsanov, *Inorg. Mater.*, 2001, **37**, 871–885).

8 R. Billing and D. E. Khoshtariya, *Inorg. Chem.*, 1994, **33**, 4038–4040.

9 Y. V. Nelyubina, K. A. Lyssenko, V. Yu. Kotov and M. Y. Antipin, *J. Phys. Chem. A*, 2008, **112**, 8790–8796.

10 Q. He, P. Tu and J. L. Sessler, *Chem*, 2018, **4**, 46–93.

11 P. Politzer, J. S. Murray, T. Clark and G. Resnati, *Phys. Chem. Chem. Phys.*, 2017, **19**, 32166–32178.

12 H. Wang, W. Wang and W. J. Jin, *Chem. Rev.*, 2016, **116**, 5072–5104.

13 S. Scheiner, *J. Phys. Chem. A*, 2021, **125**, 6514–6528.

14 A. Bauzá, T. J. Mooibroek and A. Frontera, *ChemPhysChem*, 2015, **16**, 2496–2517.

15 J. M. Holthoff, R. Weiss, S. V. Rosokha and S. M. Huber, *Chem. – Eur. J.*, 2021, **27**, 16530–16542.

16 W. Childs, *J. Phys. Chem.*, 1969, **73**, 2956–2960.

17 H. Luecke and F. A. Quiocho, *Nature*, 1990, **347**, 402–406.

18 A. A. Malär, N. Wili, L. A. Völker, M. I. Kozlova, R. Cadalbert, A. Däpp, M. E. Weber, J. Zehnder, G. Jeschke, H. Eckert, A. Böckmann, D. Klose, A. Y. Mulkidjanian, B. H. Meier and T. Wiegand, *Nat. Commun.*, 2021, **12**, 5293.

19 F. A. Kiani and S. Fischer, *J. Biol. Chem.*, 2013, **288**, 35569–35580.

20 T. Beke-Somfai, P. Lincoln and B. Nordéna, *Proc. Natl. Acad. Sci. U. S. A.*, 2011, **108**, 4828–4833.

21 W. Zhao, A. H. Flood and N. G. White, *Chem. Soc. Rev.*, 2020, **49**, 7893–7906.

22 N. G. White, *CrystEngComm*, 2019, **21**, 4855–4858.

23 M. E. Light and P. A. Gale, *CSD Commun.*, 2016, Deposition No. 1491437, Refcode: IQOKOQ.

24 M. Calabrese, A. Pizzi, R. Beccaria, A. Frontera and G. Resnati, *ChemPhysChem*, 2023, **24**, e202300298.

25 A. Daolio, A. Pizzi, G. Terraneo, A. Frontera and G. Resnati, *ChemPhysChem*, 2021, **22**, 2281–2285.

26 A. Daolio, A. Pizzi, G. Terraneo, M. Ursini, A. Frontera and G. Resnati, *Angew. Chem., Int. Ed.*, 2021, **60**, 14385–14389.

27 A. Grabarz, M. Michalczyk, W. Zierkiewicz and S. Scheiner, *Molecules*, 2021, **26**, 2116.

28 W. Zierkiewicz, M. Michalczyk, T. Maris, R. Wysokiński and S. Scheiner, *Chem. Commun.*, 2021, **57**, 13305–13308.

29 R. Beccaria, A. Dhaka, M. Calabrese, A. Pizzi, A. Frontera and G. Resnati, *Chem. – Eur. J.*, 2024, **30**, e202303641.

30 G. R. Desiraju, P. S. Ho, L. Kloo, A. C. Legon, R. Marquardt, P. Metrangolo, P. Politzer, G. Resnati and K. Rissanen, *Pure Appl. Chem.*, 2013, **85**, 1711–1713.

31 The $I_2\cdots NH_3$ adduct, probably the first synthesized σ-hole bonded system, was prepared by J. J. Colin early nineteen century: J. J. Colin, *Ann. Chim.*, 1814, **91**, 252–272.

32 G. Cavallo, P. Metrangolo, T. Pilati, G. Resnati and G. Terraneo, Halogen Bond: A Long Overlooked Interaction, in *Topics in Current Chemistry*, ed. P. Metrangolo and G. Resnati, Springer, 2015, vol. 358, pp. 1–17.

33 A. Bent, *Chem. Rev.*, 1968, **68**, 587–648.

34 The charge-transfer mindset introduced by R. S. Mulliken (ref. 35, 36), the identification of the preferred geometry of adducts involving halogens and other p block elements by N. W. Alcock (ref. 37) and R. Parthasarathy (ref. 38), the computational investigations based on electrostatics by P. Politzer (ref. 39), and the experimental findings of G. Resnati in the solid (ref. 40) gave particularly important contributions to the development of the today concept and practice of the HaB.

35 R. S. Mulliken, *J. Am. Chem. Soc.*, 1950, **72**, 600–608.

36 R. S. Mulliken, *J. Phys. Chem.*, 1952, **56**, 801–822.

37 N. W. Alcock, *Adv. Inorg. Chem. Radiochem.*, 1972, **15**, 1–58.

38 N. Ramasubbu, R. Parthasarathy and P. Murray-Rust, *J. Am. Chem. Soc.*, 1986, **108**, 4308–4314.

39 T. Brinck, J. S. Murray and P. Politzer, *Int. J. Quantum Chem.*, 1992, **44**, 57–64.

40 P. Metrangolo and G. Resnati, *Chem. – Eur. J.*, 2001, **7**, 2511–2519.

41 J. P. M. Lommerse, A. J. Stone, R. Taylor and F. H. Allen, *J. Am. Chem. Soc.*, 1996, **118**, 3108–3116.

42 C. B. Aakeroy, D. L. Bryce, G. R. Desiraju, A. Frontera, A. C. Legon, F. Nicotra, K. Rissanen, S. Scheiner, G. Terraneo, P. Metrangolo and G. Resnati, *Pure Appl. Chem.*, 2019, **91**, 1889–1892.

43 P. Scilabra, G. Terraneo and G. Resnati, *Acc. Chem. Res.*, 2019, **52**, 1313–1324.

44 A. Dhaka, I.-R. Jeon and M. Fourmigué, *Acc. Chem. Res.*, 2024, **57**, 362–374.

45 R. E. Rosenfield, R. Parthasarathy and J. D. Dunitz, *J. Am. Chem. Soc.*, 1977, **99**, 4860–4862.

46 J. S. Murray, P. Lane, T. Clark and P. Politzer, *J. Mol. Model.*, 2007, **13**, 1033–1038.

47 M. H. Kolář and P. Hobza, *Chem. Rev.*, 2016, **116**, 5155–5187.

48 P. Politzer, J. S. Murray and T. Clark, *Phys. Chem. Chem. Phys.*, 2013, **15**, 11178–11189.

49 J. S. Murray, P. Lane, T. Clark, K. E. Riley and P. Politzer, *J. Mol. Model.*, 2012, **18**, 541–548.

50 F. Weinhold, *Molecules*, 2022, **27**, 377.

51 A. K. Guha, *ChemPhysChem*, 2023, **24**, e202300403.

52 N. Tarannam, R. Shukla and S. Kozuch, *Phys. Chem. Chem. Phys.*, 2021, **23**, 19948–19963.

This journal is © The Royal Society of Chemistry 2024

Chem. Soc. Rev., 2024, **53**, 6654–6674 | **6671**

53 L. Chen, Q. Feng, C. Wang, S. Yin and Y. Mo, *J. Phys. Chem. A*, 2021, **125**, 10428–10438.

54 S. Scheiner, *Phys. Chem. Chem. Phys.*, 2023, **25**, 7184–7194.

55 J. S. Murray and P. Politzer, *ChemPhysChem*, 2021, **22**, 1201–1207.

56 K. L. C. Hunt, *J. Chem. Phys.*, 1990, **92**, 1180–1187.

57 Z. Zhu, G. Wang, Z. Xu, Z. Chen, J. Wang, J. Shia and W. Zhu, *Phys. Chem. Chem. Phys.*, 2019, **21**, 15106–15119.

58 R. F. W. Bader, *Chem. Rev.*, 1991, **91**, 893–928.

59 C. Wang, Y. Fu, L. Zhang, D. Danovich, S. Shaik and Y. Mo, *J. Comput. Chem.*, 2018, **39**, 481–487.

60 A. P. Novikov, K. E. German, A. V. Safonov and M. S. Grigoriev, *ChemistrySelect*, 2022, **7**, e202202814.

61 R. Wysokiński, W. Zierkiewicz, M. Michalczyk, T. Maris and S. Scheiner, *Molecules*, 2022, **27**, 2144.

62 D. Quiñonero, I. Alkorta and J. Elguero, *Phys. Chem. Chem. Phys.*, 2016, **18**, 27939–27950.

63 Y. Li, L. Meng and Y. Zeng, *ChemPlusChem*, 2021, **86**, 232–240.

64 J. M. Holthoff, E. Engelage, R. Weiss and S. M. Huber, *Angew. Chem., Int. Ed.*, 2020, **59**, 11150–11157.

65 W. Zierkiewicz, R. Wysokiński, M. Michalczyk and S. Scheiner, *ChemPhysChem*, 2020, **21**, 870–877.

66 Z. Yang, Z. Xu, Y. Liu, J. Wang, J. Shi, K. Chen and W. Zhu, *J. Phys. Chem. B*, 2014, **118**, 14223–14233.

67 C. Loy, J. M. Holthoff, R. Weiss, S. M. Huber and S. V. Rosokha, *Chem. Sci.*, 2021, **12**, 8246–8251.

68 F. Groenewald, C. Esterhuysen and J. Dillen, *Theor. Chem. Acc.*, 2012, **131**, 1281.

69 C. R. Groom and F. H. Allen, *Angew. Chem., Int. Ed.*, 2014, **53**, 662–671.

70 S. Scheiner, *Phys. Chem. Chem. Phys.*, 2022, **24**, 6964–6972.

71 S. J. Grabowski, *ChemPhysChem*, 2014, **15**, 2985–2993.

72 A. Ferguson, M. A. Squire, D. Siretanu, D. Mitcov, C. Mathoniere, R. Clerac and P. E. Kruger, *Chem. Commun.*, 2013, **49**, 1597–1599.

73 D. Leitz, M. C. Bayer, Y. Morgenstern, F. Zischka and A. J. Kornath, *Chem. – Eur. J.*, 2018, **24**, 15825–15830.

74 Q. Michaudel, D. Thevenet and P. S. Baran, *J. Am. Chem. Soc.*, 2012, **134**, 2547–2550.

75 P. P. Nievergelt, M. Babor, J. Cejka and B. Spingler, *Chem. Sci.*, 2018, **9**, 3716–3722.

76 S.-S. Liu, J. W. Ziller, Y.-Q. Zhang, B.-W. Wang, W. J. Evans and S. Gao, *Chem. Commun.*, 2014, **50**, 11418–11420.

77 K. Chainok, S. M. Neville, B. Moubaraki, S. R. Batten, K. S. Murray, C. M. Forsyth and J. D. Cashion, *Dalton Trans.*, 2010, **39**, 10900–10909.

78 T. Iawakiri, H. Terao, E. Lork, T. M. Gesing and H. Ishihara, *Z. Naturforsch. B*, 2017, **72**, 141–151.

79 R. Castillo, J. Cisterna, I. Brito, S. Conejeros and J. Llanos, *Inorg. Chem.*, 2020, **59**, 9471–9475.

80 M. Michalczyk, W. Zierkiewicz, R. Wysokiński and S. Scheiner, *Phys. Chem. Chem. Phys.*, 2021, **23**, 25097–25106.

81 R. Wysokiński, M. Michalczyk, W. Zierkiewicz and S. Scheiner, *Phys. Chem. Chem. Phys.*, 2021, **23**, 4818–4828.

82 S. Scheiner, R. Wysokiński, M. Michalczyk and W. Zierkiewicz, *J. Phys. Chem. A*, 2020, **124**, 4998–5006.

83 G. Resnati, D. L. Bryce, G. R. Desiraju, A. Frontera, I. Krossing, A. C. Legon, P. Metrangolo, F. Nicotra, K. Rissanen, S. Scheiner and G. Terraneo, *Pure Appl. Chem.*, 2024, **96**, 135–145.

84 K. Kamada, S.-I. Fuku-en, S. Minamide, K. Ohta, R. Kishi, M. Nakano, H. Matsuzaki, H. Okamoto, H. Higashikawa, K. Inoue, S. Kojima and Y. Yamamoto, *J. Am. Chem. Soc.*, 2013, **135**, 232–241.

85 V. Y. Lee, K. Ota, Y. Ito, O. A. Gapurenko, A. Sekiguchi, R. M. Minyaev, V. I. Minkin and H. Gornitzka, *J. Am. Chem. Soc.*, 2017, **139**, 13897–13902.

86 E. I. Davydova, A. Virovets, E. Peresypkina, A. V. Pomogaeva, A. S. Lisovenko and A. Y. Timoshkin, *Dalton Trans.*, 2021, **50**, 13357–13367.

87 J.-Q. Zhao, M.-F. Han, X.-J. Zhao, Y.-Y. Ma, C.-Q. Jing, H.-M. Pan, D.-Y. Li, C.-Y. Yue and X.-W. Lei, *Adv. Opt. Mater.*, 2021, **9**, 2100556.

88 K. Strakova, L. Assies, A. Goujon, F. Piazzolla, H. V. Humeniuk and S. Matile, *Chem. Rev.*, 2019, **119**, 10977–11005.

89 D. Fan, L. Chen, C. Wang, S. Yin and Y. Mo, *J. Chem. Phys.*, 2021, **155**, 234302.

90 Q. Ai, D. M. Williams, M. Danielson, L. G. Spooner, J. A. Engler, Z. Ding, M. Zeller, A. J. Norquist and J. Schrier, *J. Chem. Phys.*, 2021, **154**, 184708.

91 R. Takouachet, R. Benali-Cherif, E.-E. Bendeif, N. Benali-Cherif, S. Pillet and D. Schaniel, *Inorg. Chim. Acta*, 2016, **446**, 6–12.

92 N. Kamali, C. OMalley, M. F. Mahon, A. Erxleben and P. McArdle, *Cryst. Growth Des.*, 2018, **18**, 3510–3516.

93 The ''normalized contact'' Nc for an interaction between atoms i and j is the ratio Dij/(rvdWi + rvdWj), wherein Dij is the experimental separation between atoms i and j and rvdWi and rvdWj are the van der Waals radii (ref. 7) of atoms i and j. If the electron donor j is a monoatomic anion, rvdWj is substituted by the anionic radius of j (D. C. Ghosh and R. Biswas, *Int. J. Mol. Sci.*, 2003, 4, 379–407). Nc is a particularly useful way to measure the interaction separation as it allows for a more meaningful comparison of separations between different interacting atoms than the absolute values of interaction distances.

94 S. Santos dos Santos, E. Schulz Lang and G. Manzoni de Oliveira, *J. Organomet. Chem.*, 2007, **692**, 3081–3088.

95 G. A. Casagrande, E. Schulz Lang, G. Manzoni de Oliveira, S. S. Lemos and V. A. S. Falcomer, *J. Organomet. Chem.*, 2006, **691**, 4006–4011.

96 R. Wysokiński, *Phys. Chem. Chem. Phys.*, 2022, **24**, 12860–12869.

97 P. H. Svensson and L. Kloo, *Chem. Rev.*, 2003, **103**, 1649–1684.

98 K. Sonnenberg, L. Mann, F. A. Redeker, B. Schmidt and S. Riedel, *Angew. Chem., Int. Ed.*, 2020, **59**, 5464–5493.

99 Y. V. Nelyubina, M. Y. Antipin and K. A. Lyssenko, *J. Phys. Chem. A*, 2007, **111**, 1091–1095.

6672 | *Chem. Soc. Rev.*, 2024, **53**, 6654–6674

This journal is © The Royal Society of Chemistry 2024

100 K. Lamberts, P. Handels, U. Englert, E. L. Aubert and E. Espinosa, *CrystEngComm*, 2016, **18**, 3832–3841.

101 A. J. Blake, R. O. Gould, W.-S. Li, V. Lippolis, S. Parsons and M. Schroder, *Cryst. Eng.*, 1999, **2**, 153–170.

102 K. Ghosh, A. Frontera and S. Chattopadhyay, *CrystEngComm*, 2021, **23**, 1429–1438.

103 J. Short, T. J. Blundell, S. Yang, O. Sahin, Y. Shakespeare, E. L. Smith, J. D. Wallis and L. Martin, *CrystEngComm*, 2020, **22**, 6632–6644.

104 Z. Wang, Y. Cheng, C. Liao and C. Yan, *CrystEngComm*, 2001, **3**, 237–242.

105 K.-F. Tebbe and R. Buchem, *Angew. Chem., Int. Ed. Engl.*, 1997, **36**, 1345–1346.

106 J. Blake, R. O. Gould, W.-S. Li, V. Lippolis, S. Parsons, C. Radek and M. Schroder, *Angew. Chem., Int. Ed.*, 1998, **37**, 293–296.

107 F. Pan, R. Puttreddy, K. Rissanen and U. Englert, *CrystEngComm*, 2015, **17**, 6641–6645.

108 A. J. Peloquin, C. D. McMillen, S. T. Iacono and W. T. Pennington, *Chem. – Eur. J.*, 2021, **32**, 8398–8405.

109 A. Abate, M. Brischetto, G. Cavallo, M. Lahtinen, P. Metrangolo, T. Pilati, S. Radice, G. Resnati, K. Rissanen and G. Terraneo, *Chem. Commun.*, 2010, **46**, 2724–2726.

110 M. D. García, J. Martí-Rujas, P. Metrangolo, C. Peinador, T. Pilati, G. Resnati, G. Terraneo and M. Ursini, *CrystEngComm*, 2011, **13**, 4411–4416.

111 J. Martí-Rujas, L. Meazza, G. K. Lim, G. Terraneo, T. Pilati, K. D. M. Harris, P. Metrangolo and G. Resnati, *Angew. Chem., Int. Ed.*, 2013, **52**, 13444–13448.

112 K. F. Konidaris, T. Pilati, G. Terraneo, P. Politzer, J. S. Murray, P. Scilabra and G. Resnati, *New J. Chem.*, 2018, **42**, 10463–10466.

113 S. P. Kelley, H. Pei, V. Smetana, A.-V. Mudring and R. D. Rogers, *Cryst. Growth Des.*, 2020, **20**, 498–505.

114 J. Lin, J. Martí-Rujas, P. Metrangolo, T. Pilati, S. Radice, G. Resnati and G. Terraneo, *Cryst. Growth Des.*, 2012, **12**, 5757–5762.

115 K. Sonnenberg, P. Pröhm, C. Meller, H. Beckers, S. Steinhauer, D. Lentz and S. Riedel, *Chem. – Eur. J.*, 2018, **24**, 1072–1075.

116 D. Munz, J. Chu, M. Melaimi and G. Bertrand, *Angew. Chem., Int. Ed.*, 2016, **55**, 12886–12890.

117 Y. Zhang, H.-Y. Ye, H.-L. Cai, D.-W. Fu, Q. Ye, W. Zhang, Q. Zhou, J. Wang, G.-L. Yuan and R.-G. Xiong, *Adv. Mater.*, 2014, **26**, 4515–4520.

118 X.-H. Ding, S. Wang, Y.-H. Li and W. Huang, *J. Mol. Struct.*, 2015, **1079**, 266–273.

119 M. Calabrese, A. Pizzi, A. Daolio, A. Frontera and G. Resnati, *Chem. Commun.*, 2022, **58**, 9274–9277.

120 T. T. da Cunha, W. X. C. Oliveira, C. B. Pinheiro, E. F. Pedroso, W. C. Nunes and C. L. M. Pereira, *Cryst. Growth Des.*, 2016, **16**, 900–907.

121 M. A. B. Abdallah, A. Bacchi, A. Parisini, S. Canossa, P. P. Mazzeo, L. Bergamonti and S. Kamoun, *Struct. Chem.*, 2019, **30**, 1911–1928.

122 M. H. H. Wurzenberger, N. Szimhardt and J. Stierstorfer, *Inorg. Chem.*, 2018, **57**, 7940–7949.

123 T. Maxson, A. S. Jalilov, M. Zeller and S. V. Rosokha, *Angew. Chem., Int. Ed.*, 2020, **59**, 17197–17201.

124 G. Cavallo, P. Metrangolo, T. Pilati, G. Resnati and G. Terraneo, *Cryst. Growth Des.*, 2014, **14**, 2697–2702.

125 J. H. Stenlid and T. Brinck, *J. Am. Chem. Soc.*, 2017, **139**, 11012–11015.

126 A. Stepien and M. J. Grabowski, *Acta Crystallogr., Sect. B: Struct. Crystallogr. Cryst. Chem.*, 1977, **33**, 2924–2927.

127 A. Daolio, A. Pizzi, M. Calabrese, N. Demitri, J. S. Murray, P. Politzer and G. Resnati, *Cryst. Growth Des.*, 2023, **23**, 574–579.

128 M. A. Volkov, A. V. Borisov, V. G. Nenajdenko, E. A. Dukhnovsky, A. E. Bely, M. M. Grishina, A. S. Kritchenkov, R. M. Gomila, A. Frontera and A. G. Tskhovrebov, *Inorg. Chim. Acta*, 2024, **563**, 121929.

129 S. Burguera, R. M. Gomila, A. Bauzá and A. Frontera, *Crystals*, 2023, **13**, 187.

130 M. A. Volkov, A. P. Novikov, N. E. Borisova, M. S. Grigoriev and K. E. German, *Inorg. Chem.*, 2023, **62**, 13485–13494.

131 A. P. Novikov, A. V. Safonov, K. E. German and M. S. Grigoriev, *CrystEngComm*, 2024, **26**, 61–69.

132 R. Alberto, G. Bergamaschi, H. Braband, T. Fox and V. Amendola, *Angew. Chem., Int. Ed.*, 2012, **51**, 9772–9776.

133 Y.-Y. Tang, Y. Xie, Y. Ai, W.-Q. Liao, P.-F. Li, T. Nakamura and R.-G. Xiong, *J. Am. Chem. Soc.*, 2020, **142**, 21932–21937.

134 A. M. S. Riel, D. A. Decato and O. B. Berryman, *Cryst. Growth Des.*, 2016, **16**, 974–980.

135 Y. Fuma and M. Ebihara, *Acta Crystallogr.*, 2006, **E62**, m1898–m1900.

136 M. Wan, Y.-N. Wang, J.-Y. Liu, L. Tong, S.-Y. Ye, J.-Y. Li and L.-Z. Chen, *CrystEngComm*, 2022, **24**, 782–787.

137 Y. Xu, M. Calabrese, N. Demitri, A. Pizzi, T. Nag, I. Hung, Z. Gan, G. Resnati and D. L. Bryce, *Chem. Commun.*, 2023, **59**, 12609–12612.

138 J. Baldas, J. F. Boas, S. F. Colmanet, A. D. Rae and G. A. Williams, *Proc. R. Soc. London, Ser. A*, 1993, **442**, 437–461.

139 M. R. Pressprich, R. D. Willett, R. D. Poshusta, S. C. Saunders, H. B. Davis and G. L. Gardlc, *Inorg. Chem.*, 1988, **27**, 260–264.

140 C.-R. Ding, Z.-M. Jin, H.-B. Wang, M.-L. Huc and H. Lind, *Acta Crystallogr.*, 2004, **C60**, m203–m204.

141 R. Beccaria, M. Calabrese, A. Pizzi, A. Frontera and G. Resnati, submitted.

142 A. Bauzá and A. Frontera, *Chem. – Eur. J.*, 2022, **28**, e202201660.

143 C. Redshaw, M. J. Walton, D. S. Lee, C. Jiang, M. R. J. Elsegood and K. Michiue, *Chem. – Eur. J.*, 2015, **21**, 5199–5210.

144 T. Koleša-Dobravc, A. Meden and F. Perdih, *New J. Chem.*, 2015, **39**, 4265–4277.

145 M. Calabrese, R. M. Gomila, A. Pizzi, A. Frontera and G. Resnati, *Chem. – Eur. J.*, 2023, **29**, e202302176.

146 D. Quiñonero, I. Alkorta and J. Elguero, *ChemPhysChem*, 2020, **21**, 1597–1607.

This journal is © The Royal Society of Chemistry 2024

Chem. Soc. Rev., 2024, **53**, 6654–6674 | **6673**

147 D. Rottschafer, B. Neumann, H.-G. Stammler, T. Sergeieva, D. M. Andrada and R. S. Ghadwal, *Chem. – Eur. J.*, 2021, **27**, 3055–3064.

148 M. R. Buchner, M. Muller and N. Spang, *Dalton Trans.*, 2020, **49**, 7708–7712.

149 J. Pena, G. Talavera, B. Waldecker and M. Alcarazo, *Chem. – Eur. J.*, 2017, **23**, 75–78.

150 Y. V. Nelyubina, K. A. Lyssenko, A. S. Sigachev, M. Y. Antipin and A. N. Kravchenko, *Russ. Chem. Bull. Int. Ed.*, 2006, **55**, 399–407.

151 Y. V. Nelyubina, K. A. Lyssenko, D. G. Golovanov and M. Y. Antipin, *CrystEngComm*, 2007, **9**, 991–996.

152 V. Blanco, M. Chas, D. Abella, E. Pia, C. Platas-Iglesias, C. Peinador and J. M. Quintela, *Org. Lett.*, 2008, **10**, 409–412.

153 K. Otsubo, Y. Wakabayshi, J. Ohara, S. Yamamoto, H. Matsuzaki, H. Okamoto, K. Nitta, T. Uruga and H. Kitagawa, *Nat. Mater.*, 2011, **10**, 291–295.

154 D. B. Hassan, W. Rekik, A. O. Roza, F. B. Mefteh, T. Roisnel, T. Bataille and H. Naili, *Polyhedron*, 2016, **119**, 238–247.

155 C. A. Ilioudis, D. G. Georganopoulou and J. W. Steed, *CrystEngComm*, 2002, **4**, 26–36.

156 M. Murphy, A. A. E. Gaertner, A. M. Owen, S. Struder, C. D. McMillen, M. Wetzler and J. L. Brumaghim, *Inorg. Chim. Acta*, 2020, **507**, 119568.

157 A. Bauza, A. Frontera and T. J. Mooibroek, *Nat. Commun.*, 2017, **8**, 14522.

158 K. O. Christe, E. C. Curtis, D. A. Dixon, H. P. Mercier, J. C. P. Sanders and G. J. Schrobilgen, *J. Am. Chem. Soc.*, 1991, **113**, 3351–3361.

159 R. Zouari, J. M. Leger, T. Maris and N. B. Chanh, *Acta Crystallogr., Sect. C: Cryst. Struct. Commun.*, 1998, **54**, 1253–1255.

160 I. A. Efimenko, A. V. Churakov, N. A. Ivanova, O. S. Erofeeva and L. I. Demina, *Russ. J. Inorg. Chem.*, 2017, **62**, 1469–1478.

161 L. E. Pope and J. C. A. Boeyens, *J. Cryst. Mol. Struct.*, 1975, **5**, 47–58.

162 D. Paliwoda, M. Szafrański, M. Hanfland and A. Katrusiak, *J. Mater. Chem. C*, 2018, **6**, 7689–7699.

163 C. Worley, A. Yangui, R. Roccanova, M.-H. Du and B. Saparov, *Chem. – Eur. J.*, 2019, **25**, 9875–9884.

164 A. Shaikjee, D. C. Levendis, H. M. Marques and R. Mampa, *Inorg. Chem. Commun.*, 2011, **14**, 534–538.

165 A. R. Geisheimer, J. E. C. Wren, V. K. Michaelis, M. Kobayashi, K. Sakai, S. Kroeker and D. B. Leznoff, *Inorg. Chem.*, 2011, **50**, 1265–1274.

166 T. Imakubo, N. Tajima, M. Tamura, R. Kato, Y. Nishio and K. Kajita, *J. Mater. Chem.*, 2002, **12**, 159–161.

167 J. Li, Q. Feng, C. Wang and Y. Mo, *Phys. Chem. Chem. Phys.*, 2023, **25**, 15371–15381.

168 R. Wysokiński, W. Zierkiewicz, M. Michalczyk and S. Scheiner, *Phys. Chem. Chem. Phys.*, 2021, **23**, 13853–13861.

169 A. Bauzá, I. Alkorta, J. Elguero, T. J. Mooibroek and A. Frontera, *Angew. Chem., Int. Ed.*, 2020, **59**, 17482–17487.

170 M. Körfer and H. Fuess, *Zeit. Kristall.*, 1988, **183**, 27–41.

171 R. P. Sharma, A. Singh, P. Venugopalan, H. Ishihara, M. Nakashima, H. Terao and K. Horiuchi, *J. Mol. Struct.*, 2010, **973**, 27–35.

172 R. Wysokiński, W. Zierkiewicz, M. Michalczyk and S. Scheiner, *ChemPhysChem*, 2021, **22**, 818–821.

173 R. Wysokiński, W. Zierkiewicz, M. Michalczyk and S. Scheiner, *ChemPhysChem*, 2020, **21**, 1119–1125.

174 G. Wang, Z. Chen, Z. Xu, J. Wang, Y. Yang, T. Cai, J. Shi and W. Zhu, *J. Phys. Chem. B*, 2016, **120**, 610–620.

175 B. Sekula, A. Bujacz, K. Zielinski and G. Bujacz, *Int. J. Biol. Macromol.*, 2013, **60**, 316–324.

176 J. Ghuman, P. A. Zunszain, I. Petitpas, A. A. Bhattacharya and S. Curry, *J. Mol. Biol.*, 2005, **353**, 38–52.

177 R. C. Hughes, L. Coates, M. P. Blakeley, S. J. Tomanicek, P. Langan, A. Y. Kovalevsky, J. M. Garcia-Ruiz and J. D. Ng, *Acta Crystallogr., Sect. F: Struct. Biol. Cryst. Commun.*, 2012, **68**, 1482–1487.

178 T. Shinoda, H. Ogawa, F. Cornelius and C. Toyoshima, *Nature*, 2009, **459**, 446–450.

179 P. T. Nguyen, C. Deisl, M. Fine, T. S. Tippetts, E. Uchikawa, X.-C. Bai and B. Levine, *Nat. Commun.*, 2022, **13**, 5293.

180 L. M. Castro-Castro and A. M. Guloy, *Angew. Chem., Int. Ed.*, 2003, **42**, 2771–2774.

181 R. Jakubas, Z. Ciunik and G. Bator, *Phys. Rev. B: Condens. Matter Mater. Phys.*, 2003, **67**, 024103.

6674 | *Chem. Soc. Rev.*, 2024, **53**, 6654–6674

This journal is © The Royal Society of Chemistry 2024